Compact lensless digital holography

THÈSE N^{O} 8634 (2018)

PRÉSENTÉE LE 28 MAI 2018

À LA FACULTÉ DES SCIENCES ET TECHNIQUES DE L'INGÉNIEUR
LABORATOIRE DE DISPOSITIFS PHOTONIQUES APPLIQUÉS
PROGRAMME DOCTORAL EN PHOTONIQUE

ÉCOLE POLYTECHNIQUE FÉDÉRALE DE LAUSANNE

POUR L'OBTENTION DU GRADE DE DOCTEUR ÈS SCIENCES

PAR

Manon ROSTYKUS

acceptée sur proposition du jury:

Prof. C. S. Brès, présidente du jury
Prof. C. Moser, directeur de thèse
Dr Y. Emery, rapporteur
Dr B. Kemper, rapporteur
Prof. H. Altug, rapporteuse

ÉCOLE POLYTECHNIQUE
FÉDÉRALE DE LAUSANNE
Suisse
2018

To my parents...

Acknowledgements

First I would like to deeply thank Prof. Christophe Moser for giving me the great opportunity to work in his laboratory. It has been a real pleasure to work under his supervision. He always brought enthusiasm, valuable advice and support during the last four years. My gratitude also goes to Dr. Ferréol Soulez for our joint collaboration and his deep insights on phase retrieval, as well as to Mattia Rossi for his expertise with the super-resolution algorithm.

I would like to thank the team of the Laboratory of Applied Photonics Devices. I really enjoyed working and sharing moments with all of them: Zahra, Volker, Miguel, Claudia, David, Timothé, Mathieu, Enrico, Jan, Andreas, Emilio, Sébastien, Frédéric, Gaël, Salma, Maya, Philippe, Laurent, Ronald, Sunan, Babak, Chiara, and in particular my office mates: Mickaël, Eric, Damien, Paul and Dino. A distinctive thank goes to Sabrina for her help with administrative purposes and all the nice discussions we had. I feel very lucky to have been part of this group for these four years.

Thanks also to all my family and friends for all the joyful time spent together and for all the great adventures we had. A special thank you to Clément for being so supportive and enthusiastic.

Finally I would like to express my gratitude to the members of my thesis committee, Prof. Camille Brès, Prof. Hatice Altug, Dr. Yves Emery and Dr. Björn Kemper for dedicating time to read this manuscript and for being in the examination jury.

Last but not least, I would like to particularly thank my parents and my brother for their unconditional support.

Lausanne, 12 Mars 2018 M. R.

Résumé

La microscopie présente un grand intérêt pour la biologie, car elle permet d'imager des éléments qui sont trop petits pour être vus à l'œil nu. Cependant, les cellules sont pour la plupart transparentes à la lumière visible et infrarouge, ce qui les rend difficiles à voir avec un microscope traditionnel. Pour ce faire, l'imagerie de phase a été inventée par F. Zernike, qui a reçu le prix Nobel en 1953 pour cette invention. Elle fournit un contraste d'intensité pour visualiser des échantillons transparents tels que ceux trouvés en biologie sans aucune coloration. Parmi les différentes implémentations de l'imagerie de phase, la microscopie holographique numérique (DHM) est une méthode de phase bien connue qui fournit une valeur quantitative de la phase générée par l'échantillon testé.

Les implémentations de DHMs sans l'aide d'aucune lentille (dénommées "sans lentille") offrent l'avantage supplémentaire de fournir un grand champ de vision (plusieurs mm^2 comparé à plusieurs centaines de μm^2) et des configurations plus compactes que les DHMs traditionnels qui ont des objectifs de microscope de haute qualité. La résolution latérale est limitée par la taille des pixels de la caméra. Cependant, plusieurs techniques ont été développées pour obtenir une résolution sous-pixel avec des configurations sans lentille, donnant ainsi une résolution plus petite que la taille du pixel.

Dans cette thèse, deux DHMs en transmission sans lentille sont présentés en utilisant une technique d'illumination latérale afin de réduire davantage la taille du microscope et de garder un accès visuel à l'échantillon. Le premier fonctionne dans une configuration en ligne : le plus compact mais utilisant un post-traitement d'image qui prend du temps. Le second est également sans lentille et utilise une configuration hors axe permettant une imagerie en temps quasi-réel mais moins compacte. Leur utilisation pratique est décrite et des images d'échantillons transparents (phase seulement) sont montrées. Enfin, la super-résolution (sous-pixel), utilisant plusieurs hologrammes décalés d'une distance plus petite que le pixel, a été étudiée pour la configuration en ligne et démontrée sur des échantillons absorbants.

Comme ces microscopes sont compacts et constitués d'éléments peu coûteux, ils pourraient être largement répandus dans les écoles à des fins éducatives. Ils pourraient également être mis en œuvre dans des incubateurs de cellules, permettant la visualisation des processus internes à faible coût et la multiplication du nombre de mesures effectuées en même temps.

Mots-clés : microscopie, imagerie de phase, imagerie sans lentille, holographie numérique, réseaux de diffraction.

Zusammenfassung

Die Mikroskopie ist für die Biologie von großem Interesse, da sie bildgebende Verfahren ermöglicht, die zu klein sind, um mit bloßem Auge gesehen zu werden. Allerdings sind die Zellen meist transparent gegenüber sichtbarem und infrarotem Licht, wodurch es schwierig ist, diese mit einem herkömmlichen Mikroskop zu erfassen. Die von F. Zernike erfundene Phasendarstellung, für die er 1953 den Nobelpreis erhielt, bietet einen Intensitätskontrast, um transparente Proben, wie sie z.B. in der Biologie vorkommen, ohne Fleckenbildung sichtbar zu machen. Unter den verschiedenen Implementierungen der Phasenabbildung ist die digitale holographische Mikroskopie (DHM) eine bekannte Phasenmethode, die einen quantitativen Wert der Phase liefert, die von der zu untersuchenden Probe erzeugt wird.

Implementierungen von DHMs ohne die Hilfe eines Linsenelements (sog. lensless) bieten die zusätzlichen Vorteile eines größeren Sichtfeldes (mehrere mm^2 im Vergleich zu mehreren hundert μm^2) und kompakterer Setups, verglichen mit herkömmlichen DHMs und den verwendeten hochwertigen Mikroskopobjektiven. Die laterale Auflösung wird durch die Pixelgröße der Kamera begrenzt. Es wurden jedoch mehrere Techniken für linsenlose DHMs entwickelt die eine Subpixelauflösung ermöglichen.

In dieser Arbeit werden zwei linsenlose Transmissions-DHMs vorgestellt, die beide eine Seitenbeleuchtung zur Probenbeleuchtung verwenden, wodurch die Gerätegröße weiter reduziert werden kann. Die erste arbeitet in einer Inline-Konfiguration wodurch ein sehr kompakter Aufbau möglich ist, dagegen aber auch eine zeitaufwändige Bildbearbeitung erfordert. Die zweite ist ebenfalls linsenlos und verwendet eine Off-Axis-Konfiguration, was die Kompaktheit des Aufbaus zugunsten einer quasi real-time Bilderfassung aufgibt. Diese Arbeit erläutert den praktischen Nutzen der beiden Konfigurationen und belegt diesen anhand von Bildern transparenter (nur Phasen-) Proben. Zusätzlich wird die Möglichkeit der Subpixelauflösung mit mehreren, um Subpixel verschobenen Hologrammen für die Inline-Konfiguration untersucht und anhand absorbierender Proben demonstriert.

Durch den kompakten Aufbau dieser Mikroskope und die verwendeten, preisgünstigen Standardelemente, eignen sich diese ideal für den pädagogischen Einsatz in Schulen. Außerdem könnten sie in Zelleninkubatoren implementiert werden, was eine kostengünstige Visualisierung der ablaufenden Prozesse ermöglicht und gleichzeitig die Anzahl der durchgeführten Messungen verfielfacht.

Stichworte: Mikroskopie, Phasenbildgebung, Linsenlose Bildgebung, Digitale Holographie, Beugungsgitter.

Abstract

Microscopy is of high interest for biology since it allows imaging features that are too small to be seen with naked eyes. However, cells are mostly transparent to visible and infrared light which makes it difficult to see with a traditional microscope. To do so, phase imaging was invented by F. Zernike, who received the Nobel prize in 1953 for this invention. It provides intensity contrast to visualize transparent samples such as those found in biology without any staining. Among the different implementations of phase imaging, digital holographic microscopy (DHM) is a well-known phase method which provides a quantitative value of the phase generated by the sample under test.

Implementations of DHMs without the help of any lens element (so called lensless) offer the added advantage to provide large field of views (several mm^2 compared to several hundred μm^2) and more compact setups than traditional DHMs which have high quality microscope objectives. The lateral resolution is limited by the pixel size of the camera. However, several techniques have been developed to obtain subpixel resolution with lensless setups, hence giving a resolution smaller than the pixel size.

In this thesis, two lensless transmission DHMs are presented using a side illumination technique in order to further reduce the device size and keep a visual access to the sample. The first one operates in an in-line configuration: the most compact but using time-consuming image post-processing. The second one is also lensless and uses an off-axis configuration allowing quasi-real time imaging but less compact. Their practical use is described and images of transparent (phase only) samples are shown. Super-resolution (subpixel) using several subpixel shifted holograms was then investigated for the in-line configuration and demonstrated on absorptive samples.

Since those microscopes are compact and made out of off-the-shelf low priced elements, they could be broadly spread in schools for educational purposes. They could also be implemented in cells incubators, allowing visualization inside processes at low cost and multiplication of the number of measurements made at the same time.

Keywords: microscopy, phase imaging, lensless imaging, digital holography, diffraction gratings.

Contents

Acknowledgements **v**

Résumé **vii**

Zusammenfassung **ix**

Abstract **xi**

List of figures **xiv**

List of tables **xvi**

1 Introduction **1**

1.1 Basic concepts 1

1.1.1 Phase imaging 1

1.1.2 Lensless holography 8

1.1.3 Phase volume hologram gratings 11

1.2 Motivation and literature 17

1.2.1 Lensless microscopy 17

1.2.2 Superresolution 19

2 Compact lensless digital holographic microscopes **23**

2.1 In-line 23

2.1.1 Device description 24

2.1.2 Multiplexed gratings fabrication 26

2.1.3 Reconstruction algorithm 30

2.1.4 Phase imaging 32

2.2 Off-axis 36

2.2.1 Device description 36

2.2.2 Multiplexed gratings fabrication 37

2.2.3 Reconstruction algorithm 38

2.2.4 Phase imaging 38

3 Compact lensless subpixel resolution large field of view microscope **43**
3.1 Device description 43
3.2 Grating fabrication 45
3.3 Reconstruction algorithm 45
3.4 Subpixel resolution imaging 45

4 Conclusion **51**
4.1 Summary of the results 51
4.1.1 Lensless in-line digital holographic microscope 51
4.1.2 Lensless off-axis digital holographic microscope 51
4.1.3 Subpixel resolution technique for lensless microscope 52
4.2 Future work 52
4.2.1 Lensless in-line digital holographic microscope 52
4.2.2 Lensless off-axis digital holographic microscope 54
4.2.3 Subpixel resolution technique for lensless microscope 54

A Phase calibration for the in-line microscope **57**

Bibliography **70**

Curriculum Vitae **71**

List of Figures

1.1 Phase contrast microscope 2
1.2 Polarized light microscope 3
1.3 DIC microscope 4
1.4 Comparison of phase contrast, DIC and polarized light microscopies 5
1.5 TIE microscope 6
1.6 QWLSI microscope 7
1.7 Lensless in-line holography principle 8
1.8 Simulated backpropagation with an in-line hologram 9
1.9 Lensless off-axis holography principle 10
1.10 Off-axis holography reconstruction example 11
1.11 Mach-Zehnder interferometer 12
1.12 Volume hologram grating recording principle 12
1.13 Volume hologram grating reading principle 13
1.14 Angular and spectral selectivities example 14
1.15 Angular multiplexing recording principle 14
1.16 Shift multiplexing principle with two spherical reference beams 15
1.17 Microscope image of the photopolymer substrate 16
1.18 Typical photopolymer dosage response curve 16
1.19 LISA experimental set-up 18
1.20 Resolution 19
1.21 Holographic pixel super-resolution lensless on-chip microscope using a fiber-optic array 21

2.1 Waveguide device principle. 24
2.2 Compact in-line microscope scheme 25
2.3 Picture of the compact in-line microscope 26
2.4 Multiplexing recording sketch 27
2.5 Diffraction efficiency measurements setup 28
2.6 Diffraction efficiency measurements 29
2.7 Diffraction efficiency measurements with crosstalk 29
2.8 Compact in-line microscope shifts 30
2.9 Reconstructed phase with the proposed compact in-line digital holographic microscope 33

2.10 Reconstructed phase with one in-line digital hologram 34
2.11 Reconstructed phase with and without regularization 34
2.12 Resolution of the proposed compact in-line digital holographic microscope . . 35
2.13 Compact off-axis microscope scheme 37
2.14 Reconstructed phase (full FOV) with the proposed compact off-axis digital holographic microscope 39
2.15 Resolution of the proposed compact off-axis digital holographic microscope . . 40
2.16 Reconstructed phase with the proposed compact off-axis digital holographic microscope 41

3.1 Compact lensless subpixel resolution large field of view microscope 44
3.2 Wavelength shift VS. driving current of the VCSEL 44
3.3 Subpixel shift principle 45
3.4 Sketch of the subpixel shifts directions 45
3.5 Reconstructed amplitude with the proposed compact subpixel resolution microscope 47
3.6 Sketch of the two superimposed sample experiment 48
3.7 Reconstructed amplitude at different depths with the proposed compact subpixel resolution microscope 49

4.1 Sketch of the proposed compact lensless in-line digital holographic microscope using a ring light source 53
4.2 Sketch of the proposed fluorescence compact lensless in-line digital holographic microscope 53
4.3 Compact lensless ultra large field of view subpixel resolution microscope 55

A.1 Calibration curve 57
A.2 Reconstructed phase from two different field of views with the proposed compact in-line digital holographic microscope 58
A.3 Reconstructed phase from two different samples with the proposed compact in-line digital holographic microscope 58

List of Tables

2.1 Multiplexing exposure times 27

3.1 Hologram shifts for different VCSEL driving currents 46

1 Introduction

Microscopy is a well-known imaging technique that encompasses many different modalities, such as for example bright field, fluorescence, phase contrast and confocal. It allows to observe elements that are too small to be seen by naked eyes.

In this thesis, new compact lensless microscopes are described. In order to achieve compact and cost-efficient microscopes, analog and digital holography techniques are exploited for imaging without lenses. First phase microscopes have been developed and then a technique to increase the spatial resolution in such microscopes has been explored.

In this introduction the basic concepts utilized in the thesis and the state of the art of the topic are described.

1.1 Basic concepts

1.1.1 Phase imaging

Imaging transparent objects is an important challenge for biology since cells are mostly transparent to visible and infrared light. Phase imaging allows imaging such objects without any prior staining of the sample. Different modalities exist. Phase contrast microscopy [1], polarized light microscopy [2] and differential interference contrast (DIC) microscopy [3] are three of the most spread techniques. They will be detailed in the following.

Phase contrast microscopy

Phase contrast microscopy is based on the conversion of the phase change caused by the transparent sample, into an intensity change that can be observed by eye or with a camera. The sample is illuminated by a hollow cone. It creates a phase shift of the incident light due to its thickness and refractive index. In order to create destructive (or constructive) interferences between the diffracted light from the sample and the directly transmitted light, the directly

transmitted light is then phase shifted by a phase ring, as shown in Figure 1.1. Interferences can be seen by naked eye or visible camera. The result is an image with dark (resp. bright) features on bright (resp. dark) background.

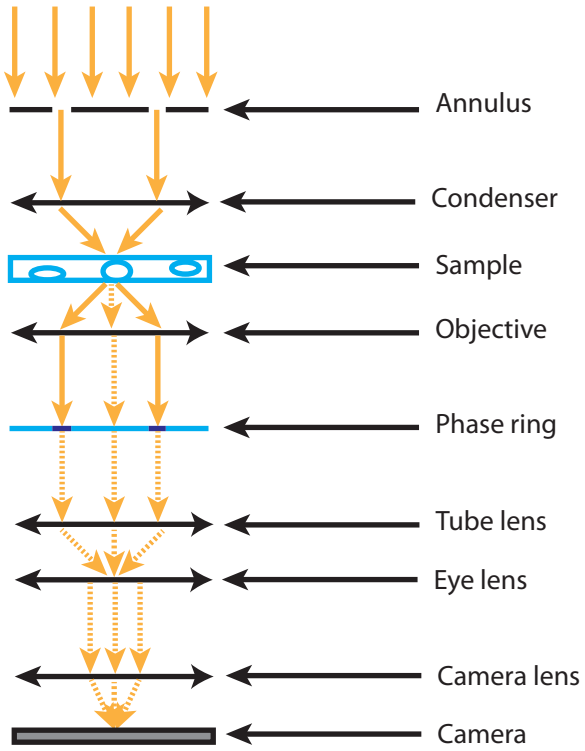

Figure 1.1 – Phase contrast microscope scheme.

This technique is useful for birefringent samples or sample holders since it does not use any polarization property. Halos artifacts are typical of this technique. However it is not recommended to image thick samples because of the lack of z-sectioning.

Polarized light microscopy

The beam from the light source is linearly polarized before the sample. The light going through phase changes inside the sample undergoes a polarization change. A crossed-polarizer is placed after the sample to block the directly transmitted light, as shown in Figure 1.2. This technique is useful for imaging birefringent samples (ones that have a refractive index depending on the incident light polarization). This technique does not have halos artifacts as encountered in phase contrast images.

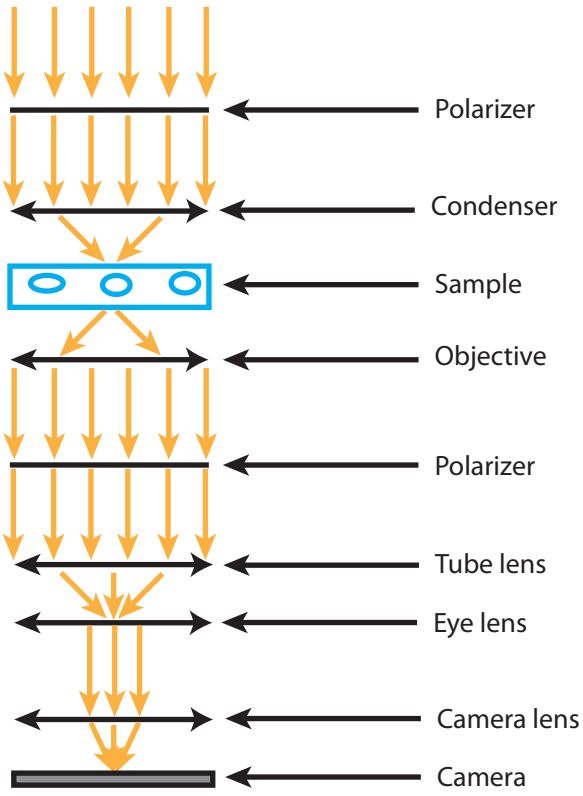

Figure 1.2 – Polarized light microscope scheme.

Differential interference contrast microscopy

In DIC microscopy, the incident beam is split in two beams with orthogonal polarizations and spatially separated by a distance smaller than the microscope lateral resolution. Both beams illuminate the sample and are recombined to create interferences, as shown in Figure 1.3. The optical path differences encountered by both beams are visible in the interference image. So DIC microscopy converts phase gradient into intensity.

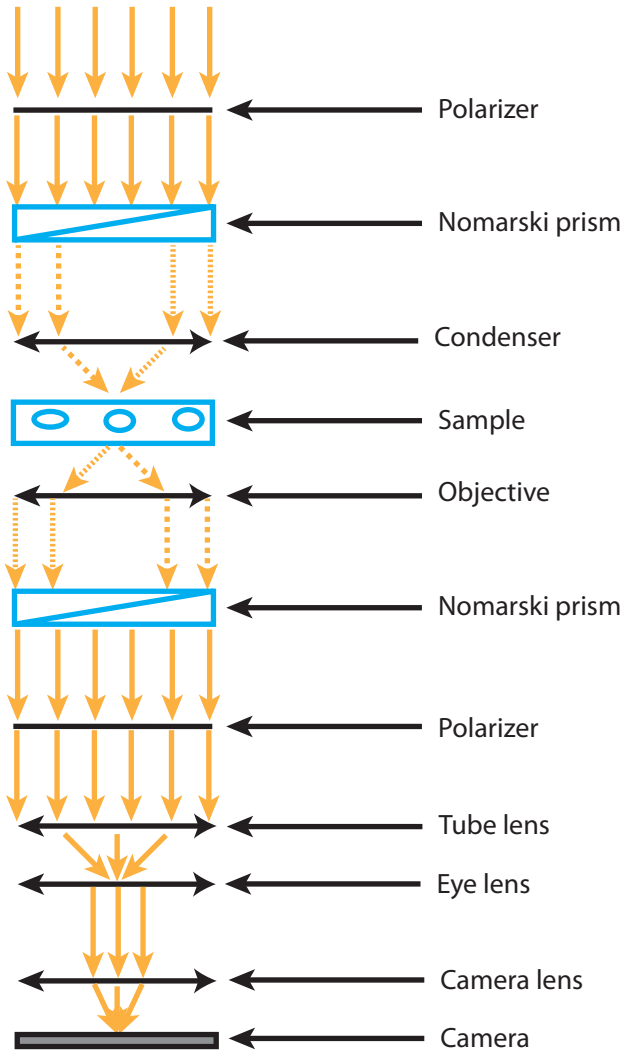

Figure 1.3 – DIC microscope scheme.

Compare to phase contrast microscopy, no phase stop is used so the full NA of the objective is used which results in a better resolution and a z-sectioning enabling thick sample imaging. Moreover, there is no halo artifact. However, this technique is not suitable for birefringent samples or sample holders. Finally, shadowing in the shearing direction (due to the contrast which is proportional to the optical path gradient) should not be interpreted as an estimation of height.

Without additional modifications, these techniques do not give quantitative information about the phase shift, i.e. the optical thickness of the cell (the product of index of refraction by the cell thickness); they only allow visualization.

Figure 1.4 shows a comparison of these three techniques:

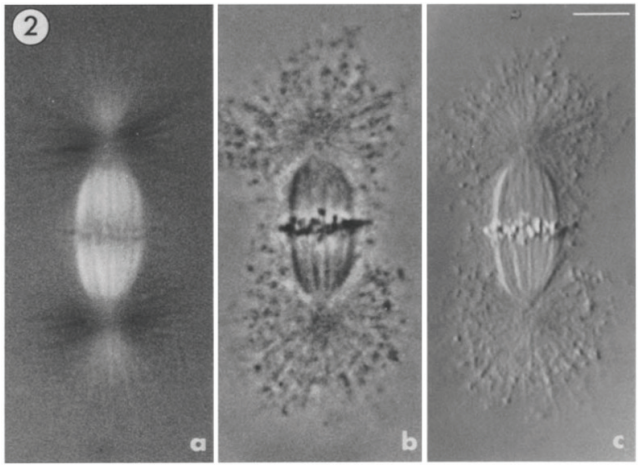

Figure 1.4 – Isolated spindle at early metaphase viewed with (a) polarization, (b) phase-contrast, and (c) differential interference contrast microscopy . Scale bar = 10µm. Reproduced from [4].

Transport of intensity equation approach

The transport of intensity equation (TIE) approach is based on the recording of several defocused images of the sample illuminated with incoherent light (e.g. white light) [5], as shown in Figure 1.5. TIE is used to express the propagation of the light between the different planes of defocus [6, 7]. It allows to reconstruct the quantitative phase and amplitude of the sample. Uniform intensity illumination can be easily achieved using a white light source. If the optical field at a given z is considered:

$$U(x,y) = \sqrt{I(x,y)}\exp^{i\phi(x,y)} \tag{1.1}$$

where $I(x,y)$ is the intensity and $\phi(x,y)$ is the spatial phase distribution. Then in the paraxial approximation the TIE is [6]:

$$k_0 \frac{\partial I(x,y)}{\partial z} = -\bigtriangledown [I(x,y) \bigtriangledown \phi(x,y)] \tag{1.2}$$

where $k_0 = \frac{2\pi}{\lambda}$ is the wave number and λ is the spectrally-weighted mean wavelength of illumination. The intensity is obtained by recording an image at focus plane and the z-derivatives are obtained by defocusing the image.

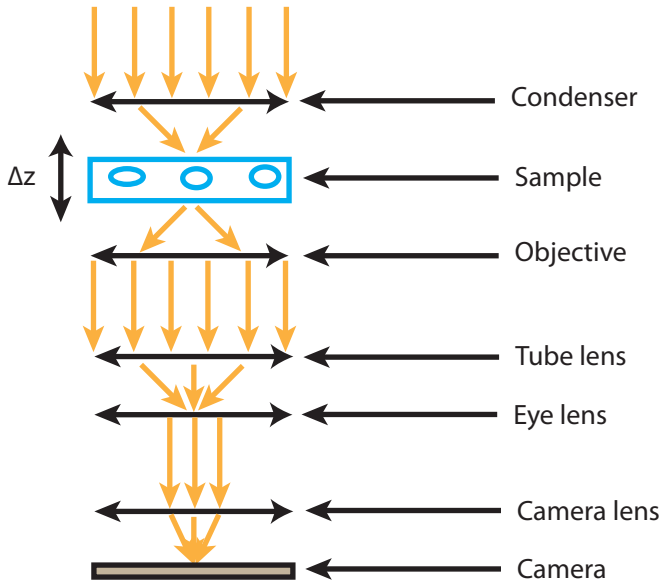

Figure 1.5 – TIE microscope scheme.

Lateral shearing interferometry

In lateral shearing interferometry, the sample is illuminated in transmission and then the wavefront after the sample is replicated and the replica is shifted laterally. Both interfere on a camera, as shown on Figure 1.6. The phase gradients are retrieved by specific algorithms [8]. However, when the lateral shear is performed in only one direction, the recovered gradient is also in the same direction so no quantitative 2D phase is retrieved. That is why quadriwave lateral shearing interferometry (QWLSI) was developed [9]. In this case, the wavefront after the sample is replicates 4 times with each time a different lateral shift in different direction. Two gradients along two different directions are reconstructed and combined to create a quantitative phase image. This technique can be implemented in a classical microscope.

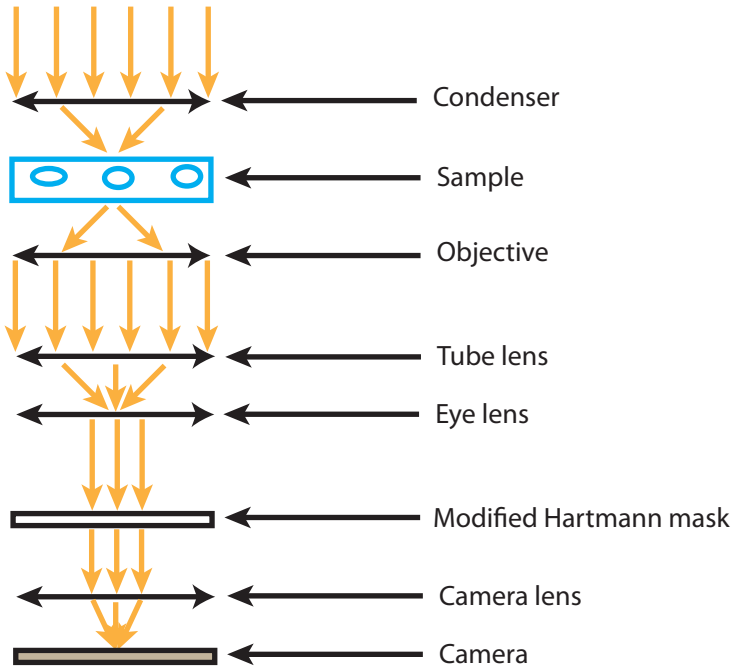

Figure 1.6 – Quadriwave lateral shearing interferometric microscope scheme. The modified Hartmann mask, which is a 4-wave-only 2D diffraction grating, is used to create the replica.

Digital holographic microscopy

Digital holographic microscopy (DHM) is based on recording a hologram of the sample. The latter is then reconstructed digitally in order to retrieve the amplitude and phase of the sample. It is a quantitative phase imaging technique, which means that transparent objects cannot only be visualized but quantitative information about the optical thickness (i.e. morphology) can be extracted with nanometer precision [10–17]. It is thus a label-free method which does not require the kind of staining used in fluorescent microscopy [18]. The DHM technique also allows for real time data recording, such as to view the damage or the repair of cells in real time during laser microsurgery [19], observe cell division [20] or changes of cellular volume to monitor apoptosis for example [12, 13, 21–24]. During the digital image reconstruction, the object can be retrieved at different focal planes which makes 3D tracking of particles/cells possible [10, 25–29]. The observation of neuronal network activity also paves the way to functional imaging using DHM [30]. Finally biophysical parameters are accessible such as intra cellular refractive index [12, 13, 22, 23] and dried mass concentration [31].
The DHM technique has been chosen in the present work because of its capacity to retrieve the quantitative phase and the fact that it can be designed in a lensless, cost-effective and compact way. More details will be given in the next section.

1.1.2 Lensless holography

Holography is an interferometric technique that consists in encoding amplitude and phase information of a sample in an intensity pattern called an hologram. In this technique, the sample is illuminated with a coherent or partially coherent light, e.g. from a laser. This beam is called object beam and contains information about the sample. A second beam, coherent with the first one, is used as reference and does not contain sample information. The hologram H is the interference between the reference beam R and the object beam O. H can be written as:

$$H = RR^* + OO^* + RO^* + OR^* \tag{1.3}$$

where * means conjugate. The interference terms RO^* and OR^* contain the virtual and real images. The goal of this technique is to retrieve the amplitude and phase of one of these two images. The basic idea is to isolate one of the interference term and then propagate it through a distance equal to the one between the sample and the recording medium (i. e. the camera in case of digital holography). This allows to know how the sample disturbed the light, hence know the amplitude and phase of the sample. This kind of process is well-known and called backpropagation [17,32,33]. Different types of holography exist. In this manuscript, I will only focus on: lensless in-line and off-axis holographies in transmission.

In-line

In lensless in-line holography, the light is decomposed in two beams after the sample: one disturbed and one undisturbed as shown in Figure 1.7. The disturbed beam is the part of the light that has been scattered by the sample: it is the object beam; and the undisturbed part is the part of the light that goes through without "seeing" the sample: it is the reference beam. Both interfere at the camera plane. This interference pattern is sampled and digitized by the camera chip to give the so-called digital in-line hologram.

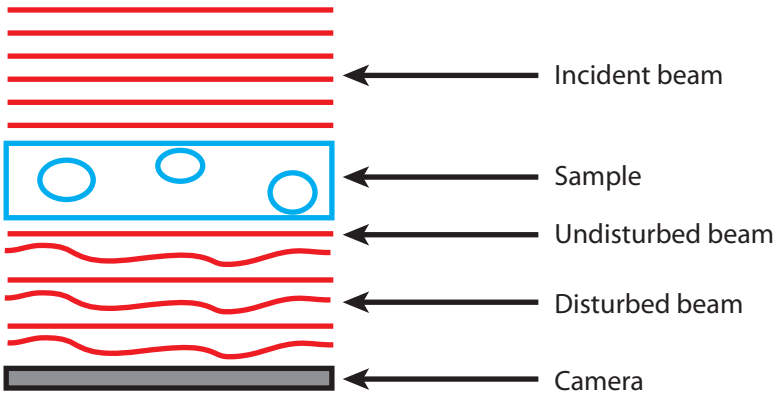

Figure 1.7 – Lensless in-line holography principle scheme. An incident beam illuminates the sample. After the sample the undisturbed beam and the disturbed beam interfere on the camera. An in-line hologram is then recorded.

In order to unambiguously retrieve the quantitative amplitude and phase of the sample from in-line holograms, a phase retrieval algorithm is required [17, 32] which uses more than one hologram. This is due to the well-known twin-image problem, characteristic of in-line holography. Indeed, the real, virtual and zero order images are superimposed in the spectrum, which implies that the image is disturbed by the out-of-focus twin-image [17] and the phase cannot be retrieved correctly. This twin-image problem arises from the intensity-only measurements and the subsequent loss of the phase. Figure 1.8 shows a simulation of in-line holography. The ground truth consists of dried human epithelial cells on a microscope slide that have been imaged using a commercial digital holographic microscope (DHM) from LynceeTec. The reconstructed amplitude and phase of the cells measured with the DHM are then used to simulate in-line holography. Figure 1.8(a) is the original amplitude and Figure 1.8(b) is the original phase. These two are combined to make a simulated hologram. Figure 1.8(c) (resp. Figure 1.8(d)) shows the reconstructed amplitude (resp. phase) using only backpropagation of one hologram. The twin image is clearly visible creating ringing structures around objects.

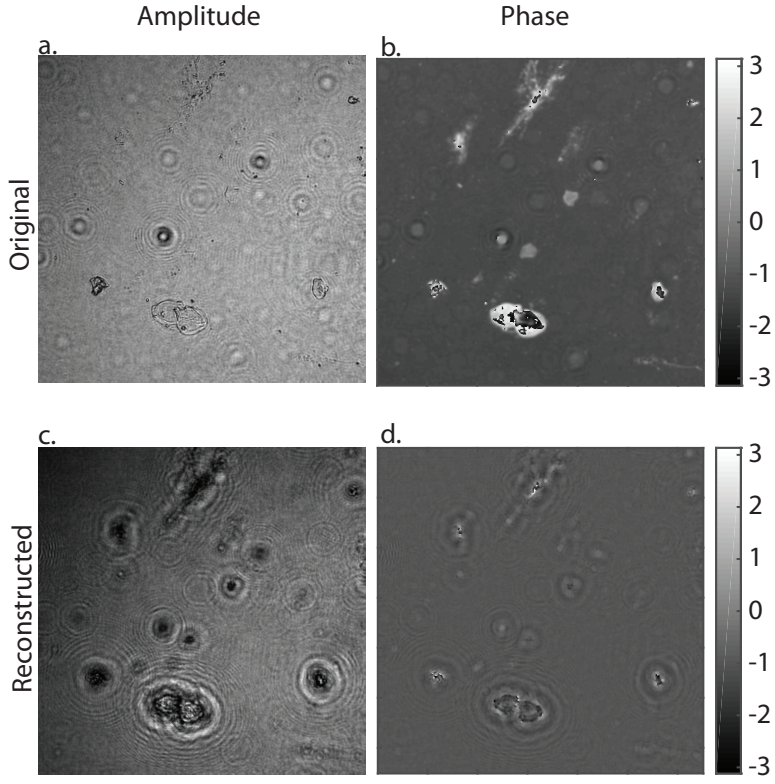

Figure 1.8 – Simulated backpropagation with an in-line hologram using dried human epithelial cells on a microscope slide imaged with a commercial DHM from LynceeTec as simulated object. (a) Original object amplitude. (b) Original object phase. (c) Reconstructed amplitude using backpropagation algorithm with only one simulated hologram. (d) Reconstructed phase using backpropagation algorithm with only one simulated hologram. Color bars are in radians.

This twin image problem is solved numerically by the mean of phase retrieval algorithms. They estimate both phase and amplitude from intensity-only holograms using additional information. This can be prior knowledge about the sample as support constraints [34–38]. The required information can also be gathered by recording several holograms of the same sample with, for instance, different distances between the sample and the camera [39, 40], different light source wavelengths [41], or by illuminating the sample with different illumination directions [42]. Finally, phase-shifting is another way to retrieve the phase in in-line holography [43, 44]. This technique consists in recording four digital in-line holograms with each time a phase shift of the reference beam.

Off-axis

Another way to avoid the twin-image problem is to use lensless off-axis holography. This technique consists in illuminating the sample with one beam that interferes coherently with a second beam that does not go through the sample and makes an angle with the first beam as shown in Figure 1.9.

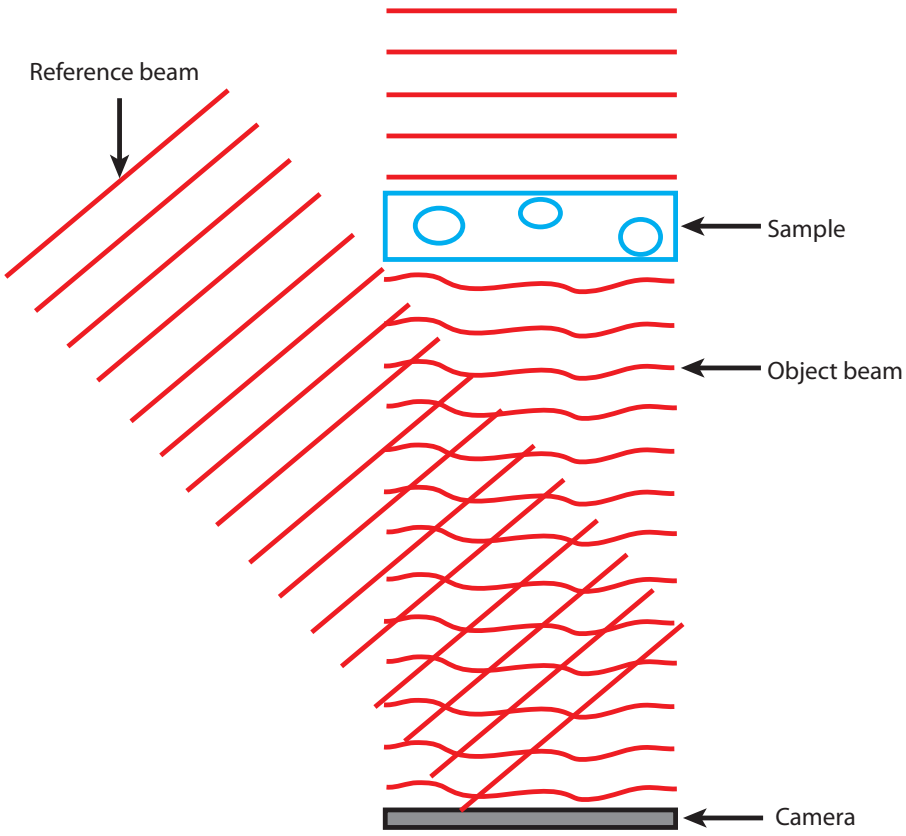

Figure 1.9 – Lensless off-axis holography principle scheme. An incident beam illuminates the sample. The object beam and the reference beam, that did not go through the sample and is coherent with the object object, interfere on the camera. An off-axis hologram is then recorded.

The angle between the two beams acts as a carrier spatial frequency. The real image, virtual image and zero order are then separated in the spectrum, as depicted in Figure 1.10(b). This spectrum is filtered to isolate the real (or virtual) image as shown in Figure 1.10(c). This step allows retrieving a twin-image free image. Finally, the correct phase is obtained using backpropagation algorithm [17, 32, 33] on the image corresponding to the filtered spectrum.

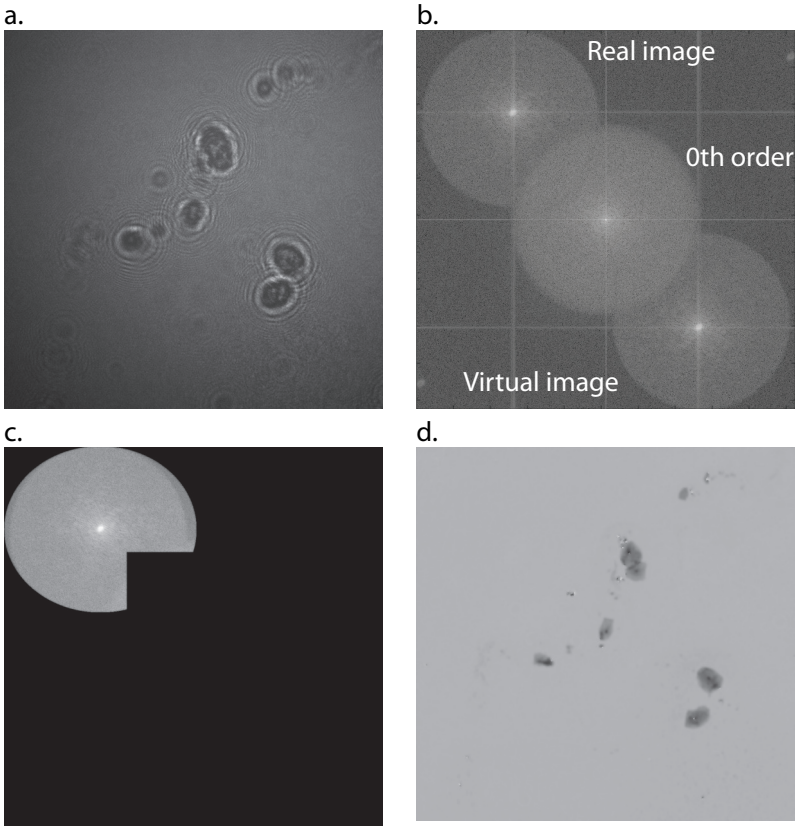

Figure 1.10 – Off-axis holography reconstruction example.(a) Hologram of dried epithelial human cells recorded with a commercial DHM with a 5x objective. (b) Spectrum of (a). (c) Filtered spectrum (i.e. filtered (c)). (d) Reconstructed phase from (a) after backpropagation from the inverse Fourier transform of (c).

1.1.3 Phase volume hologram gratings

In this thesis phase volume hologram gratings are used to shape and redirect an incident light beam. In order to record the hologram gratings, a Mach-Zehnder interferometric setup is used. A continuous wave, single frequency laser is collimated and split by a beam splitter to generate a signal beam and a reference beam. The reference and the signal beams interfere in the photopolymer and induce a change of refractive index, which results in a phase volume grating. A basic scheme of such interferometer is shown in Figure 1.11.

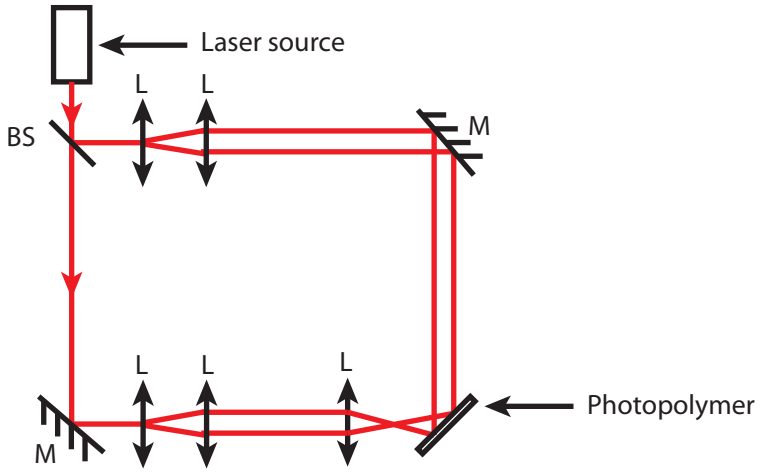

Figure 1.11 – Mach-Zehnder interferometer scheme. M = mirror. BS = beam splitter, L = lens.

Figure 1.12 shows an example of recording.

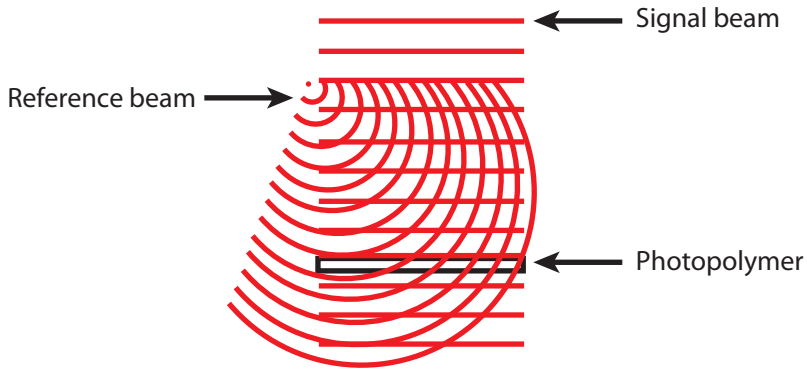

Figure 1.12 – Volume hologram grating recording principle scheme. The signal beam and the reference beam interfere in the photopolymer. Its refractive index changes according to the amount of light it receives. After this exposition, the photopolymer is illuminated with a white light in order to fix the grating.

After recording, the photopolymer is cured using white light in order to fix the grating inside the photopolymer. Then when the grating is illuminated with the same reference beam, the diffracted light will be shaped and redirected similarly to the signal beam, as shown in Figure 1.13.

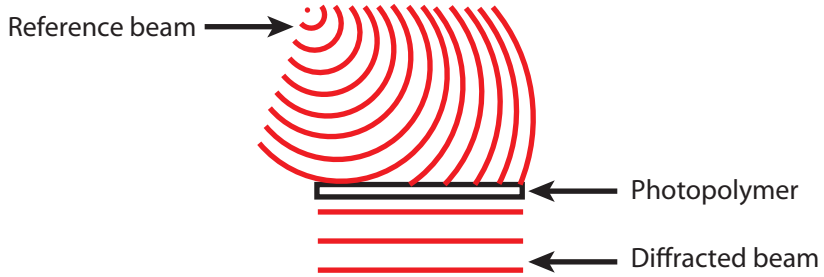

Figure 1.13 – Volume hologram grating reading principle scheme.The reference beam (same as the one used in the recording process) illuminates the grating and is then shaped and redirected as the signal used in the recording process.

Multiplexing

Each grating is characterized by the Bragg condition:

$$\vec{k_r} - \vec{k_d} = \vec{G} \tag{1.4}$$

where $\vec{k_r}$ is the reference beam wave vector, $\vec{k_d}$ is the diffracted beam wave vector and $\vec{G}$ is the grating vector. The diffracted beam then depends on the reference beam incident angle and wavelength. This property is used to multiplex holograms, i.e. to record several holograms in the same volume of the photopolymer. Indeed, when the Bragg condition is no more fulfilled, the diffraction efficiency of the diffracted beam goes to zero, which means that there is no more diffracted beam. So if several holograms are recorded with different Bragg conditions, they will be multiplexed and only one beam will be diffracted per reference beam. The diffraction efficiency in a transmission grating can be written as [45]:

$$\eta = \frac{sin^2(\nu^2 + \xi^2)^{\frac{1}{2}}}{1 + \frac{\xi^2}{\nu^2}} \tag{1.5}$$

where

$$\xi = \frac{\Delta\theta K d sin(\phi - \theta_0)}{2c_s} = \frac{-\Delta\lambda K^2 d}{8\pi n c_s} \tag{1.6}$$

and

$$\nu = \frac{\pi n_1 d}{\lambda (c_r c_s)^{\frac{1}{2}}} \tag{1.7}$$

where $c_r = cos(\theta)$ and $c_s = cos(\theta) - \frac{K}{\beta} cos(\phi)$ are the obliquity factors, ϕ the slant angle of the grating, $\beta = \frac{2\pi n}{\lambda}$, K = $\frac{2\pi}{\Lambda}$ the grating vector, Λ the grating period, n_1 refractive index modulation, d the thickness of the grating, $\Delta\theta$ the angular deviation from the Bragg angle θ_0, $\Delta\lambda$ the spectral deviation from the Bragg wavelength λ_0.

Figure 1.14 shows typical efficiency curves with respect to the angular deviation (Figure 1.14(a)) and spectral deviation (Figure 1.14(b)) for a transmission grating of thickness 70μm.

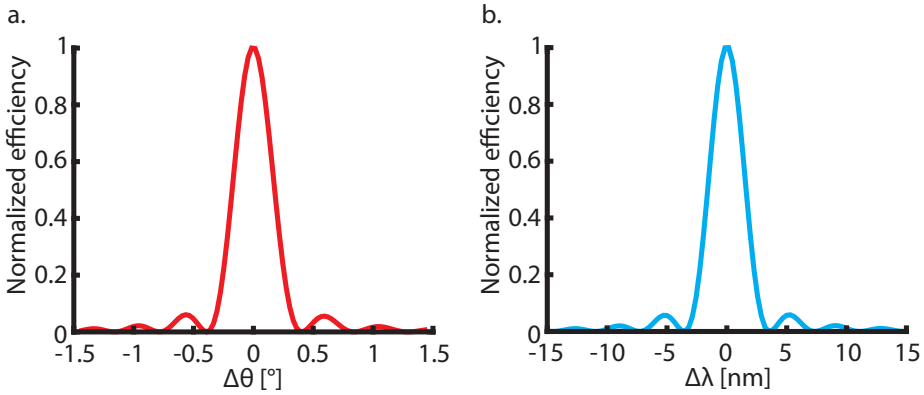

Figure 1.14 – (a) Angular selectivity and (b) spectral selectivity for a transmission grating assuming $\theta_0 = 60°$, $\lambda_0 = 681nm$, $n_1 = 10^{-3}$, $n = 1.5$, $\Lambda = 0.5\mu m$, $\phi = 1.4 radian$ *and* $d = 70\mu m$.

The angular selectivity at Full Width Half Maximum (FWHM) of a transmission grating can be approximated by [45]:

$$\Delta\theta_{FWHM} = \frac{\Lambda}{d} \tag{1.8}$$

Similarly the wavelength selectivity at Full Width Half Maximum (FWHM) of a transmission grating can be approximated by [45]:

$$\Delta\lambda_{FWHM} = \lambda cot(\theta)\frac{\Lambda}{d} \tag{1.9}$$

Multiplexing can be done in different ways [46] such as angularly (different incident angles for each reference beam), as depicted in Figure 1.15, or spectrally (difference wavelengths for each reference beam).

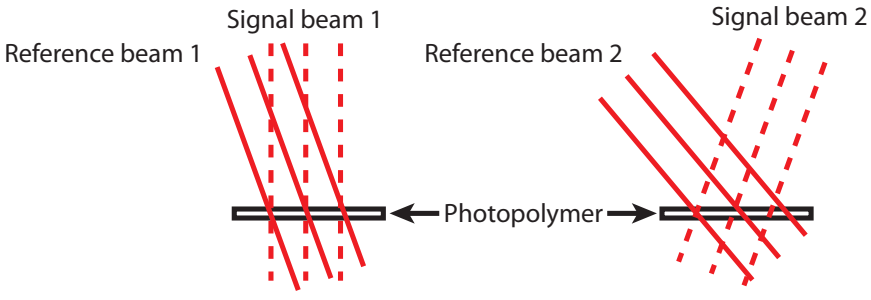

Figure 1.15 – Angular multiplexing recording principle. Recording of only two multiplexed gratings is shown for clarity. The recording of the first grating is done by exposing the photopolymer to reference beam 1 and signal beam 1. The recording of the second multiplexed grating is done by exposing the same photopolymer to reference beam 2 and signal beam 2.

However, if the Bragg condition mismatch between two gratings is not fulfilled, cross-talk will appear. Cross talk is the effect of having several diffracted beams corresponding to a single reference beam. Depending on the application this can be a limitation and needs to be minimized. The angular (respectively spectral) selectivity needs to be measured in order to evaluate the angular or spectral shift necessary to achieve a given cross-talk value.

Shift multiplexing

It is important to note that angular multiplexing can be done by using a spherical wave instead of a plane wave, a multiplexing scheme coined shift multiplexing. Indeed, as depicted in Figure 1.16, when a spherical reference beam is moved, the incident angle on a specific point varies [47]. This is the multiplexing technique used in this thesis. When several hologram gratings are recorded sequentially in the same volume of the photopolymer, the level of light exposure seen by each hologram depends on the order in which they were recorded, as shown in Figure 1.16. Hence a so called exposure schedule needs to be devised in order to match the diffraction efficiency of each hologram.

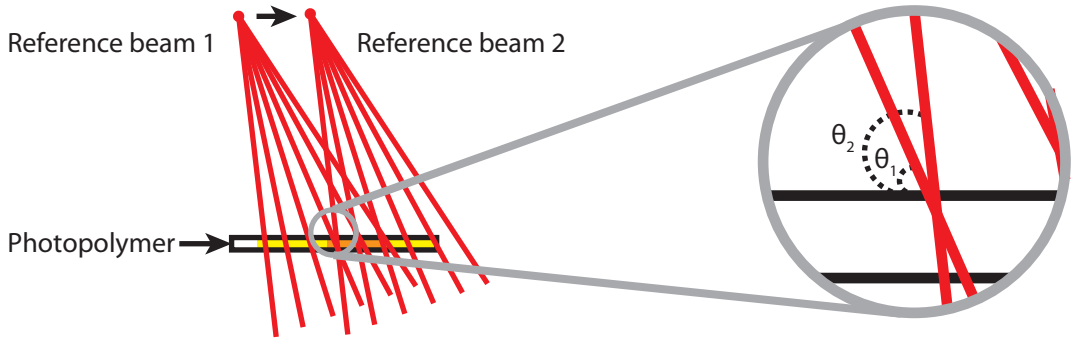

Figure 1.16 – Shift multiplexing principle with two spherical reference beams. Only two reference beams are shown for clarity. The photopolymer is exposed by both reference beams on the orange region and only one on the yellow regions. On the left, a zoom of the overlapping part of the photopolymer shows the incident angle difference between the two shifted beams on a specific point.

Photopolymer material

The photopolymer material also affects the beam homogeneity. Indeed, in this thesis the photopolymer has defects inside its volume, as can be seen in Figure 1.17, which create unwanted diffraction patterns in the diffracted beam. Moreover, only one side of the photopolymer was protected by a cellophane removable layer. The other side of the photopolymer could be scratched during the multiple preparation of the samples. The combination of volume scattering defects and surface aspect further create a spatial beam inhomogeneity.

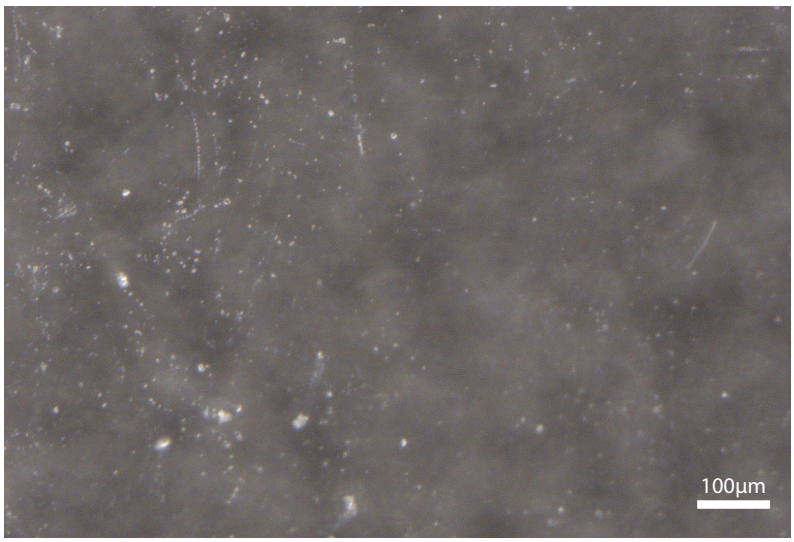

Figure 1.17 – Microscope image of the photopolymer substrate, taken with a reflection widefield microscope. Defects are visible in white on the image.

However, it has been chosen because it is very easy to use (laminated directly onto a glass holder and fast curing with white light), adapted to the red source wavelength (670nm) and with enough dynamic range ($\Delta n \approx 10^{-3}$) for multiplexing several holograms with good efficiency for my experiments.
Moreover, the recording process is as follow. The polymerization starts when the photopolymer is first exposed to light and only stops when all the polymerizable monomers are consumed [48]. While recording a grating, the monomers diffuse to the bright fringes of the interference pattern and polymerize. This diffusion creates the refractive index of the material to be modulated [48]. Finally, the photopolymer has first to be exposed with uniform incoherent precure light in order to reach the polymerization threshold uniformly [48], as depicted in Figure 1.18, so that the subsequent exposure produce a linear change of index with exposure dose [48].

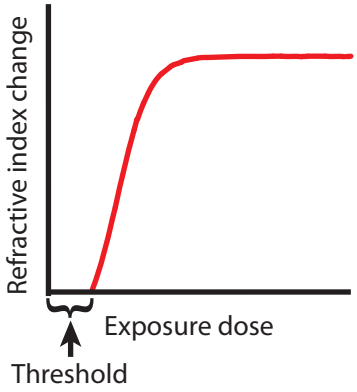

Figure 1.18 – Typical photopolymer dosage response curve.

1.2 Motivation and literature

1.2.1 Lensless microscopy

Lensless imaging refers to an imaging technique which requires no imaging element, such as microscope objective, between the light transmitted by the sample and the camera [49]. This configuration enables designing compact devices. It was initially developed for imaging in the Xray and UV spectral ranges because of the difficulty to produce lenses in these wavelength ranges [50]. In the visible range, it is mainly investigated for microscopy, because lensless imaging provides high resolution (sub-micrometer) with a large field of view (FOV) equal to the size of the camera chip (~several mm^2). In classical microscopy, the FOV is limited by the magnification and the camera chip size as:

$$FOV = \frac{\text{camera chip size}}{\text{magnification}} \tag{1.10}$$

Moreover, lensless microscopy also has the advantage to be cost effective since microscope objectives are expensive and bulky. DHM has also been developed without any microscope objective or lenses in order to obtain a simpler setup. Those devices are made of the same three parts as a classical microscope: illumination, a sample on a slide and a detector; however the detection part only contains a camera; no optical element is situated between the sample and the camera.

In-line digital holography

In-line DHM has been well investigated as a lensless interferometric technique for phase imaging, which requires only one illumination beam. This technique has been proposed with incoherent illumination [49,51–57] to create speckle-free images; however, the compactness of the imager is then compromised since a rather large distance (several centimeters) is needed between the source and the sample to obtain enough spatial coherence. Other compact common-path interferometric methods have been investigated to obtain quantitative phase imaging based on lateral phase shifting [58,59]. In digital in-line holography, the quantitative phase cannot be retrieved by only applying backpropagation to the recorded hologram as explained in 1.1.2. One of the phase retrieval technique uses a multi-angle illumination [42,60]. During this process, several holograms are recorded with different illumination directions. The amplitude and the phase are then numerically reconstructed using all those holograms. This technique has been proposed with an optical fiber mounted on a rotational arm [42,54] as shown in Figure 1.19 or several light-emitting diodes (LEDs) coupled in a fiber-optic array [61]. In this system, the distance between the end of the fiber and the object has to be quite large (several cm) to obtain enough spatial coherence. Moreover, the illumination is placed on top of the sample, which makes difficult additional measurements such as fluorescence imaging. This multi-angle illumination can also be used to resolve depth in a volume [41,62,63].

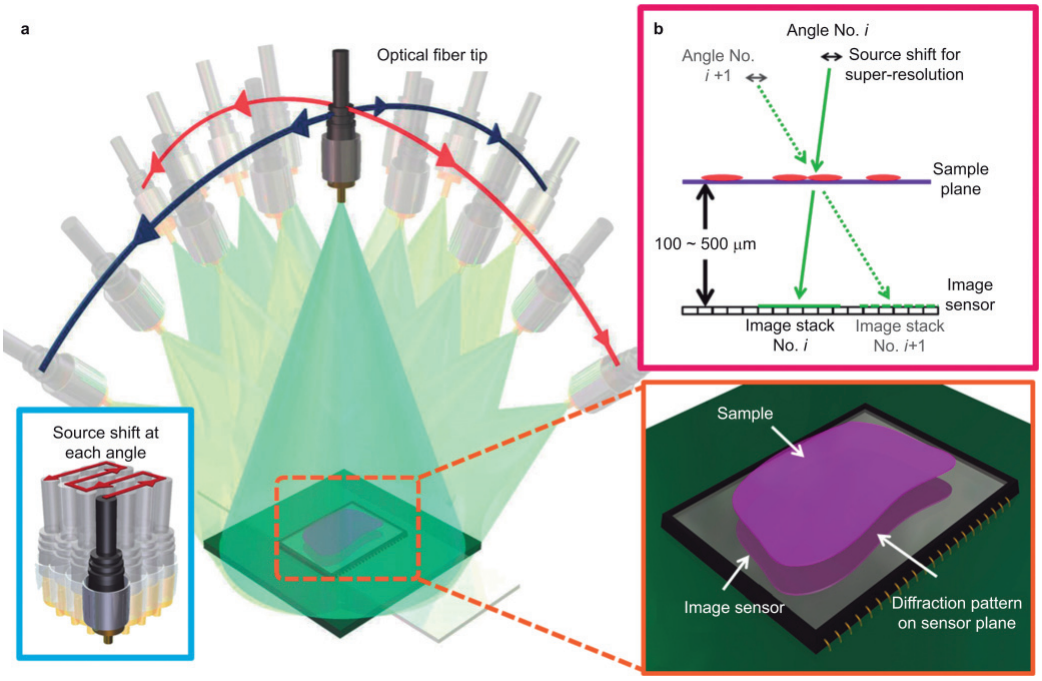

Figure 1.19 – LISA, Lensfree Imaging using Synthetic Aperture, experimental set-up. (a) A partially coherent light source (spectral bandwidth:,2.5 nm) is coupled to a single mode fiber. This fiber is mounted on a rotational arm to provide tilted illumination across two orthogonal axes (red and blue trajectories). At each angle, the source is laterally shifted multiple times (see bottom left inset) to capture a stack of lower-resolution holographic images. (b) The sample is placed onto the image sensor chip at a distance of about 100–500 µm. The distance between the fiber end and the image sensor is about 7–11 cm. Reproduced from [42]

Off-axis digital holography

When applied to microscopy, off-axis DHM is often used to image transparent biological material and quantify the optical thickness of cells [14, 64–70], since a quantitative measurement of the phase is accessible. Diverse implementations have been presented such as an add-on for a widefield microscope [71–73], a color DHM [74], autofocus [75], as a portable device that uses a grating to redirect part of the incident light to create a reference beam with a specific angle [76, 77] and stand-alone DHM in transmission and reflection configuration [78]. Reconstruction can be done in different depth planes which allows DHM to track elements in a 3D volume [69, 79, 80]. Tomography has also been investigated by rotating the sample and recording several holograms [81, 82]. Compact versions of off-axis DHMs have been implemented [83–85]. For example, an implementation makes use of a beam splitter to obtain two beams, object and reference, from one light source [83, 86]. An objective is added in front of the sample to increase the resolution. This type of design only works in reflection. Another proposed scheme is made of a set of different lenses to image in transmission [84]. The two paths are created by using only a part of a collimated beam for each beam (object and

reference). Finally, other holographic techniques have been utilized to achieve this goal, such as self-interference design [85,86] and shearing interferometry [87]. All those implementations either include lenses or only work in reflection.The same kind of device using a beam splitter has been presented for lensless imaging [88], i.e. without an objective in front of the sample, which makes it more compact but works only in reflection.

1.2.2 Superresolution

Resolution and contrast

The resolution of an image is defined by the shortest distance between two points that can be distinguished. The Rayleigh criterion is often used as resolution of an optical system. It corresponds to the distance between two Airy functions (which are the impulse responses of an optical system with a circular aperture) when the first zero of the first one coincides with the maximum of the second one, as shown on Figure1.20 with:

$$I(x) = (\frac{2J_1(\pi x)}{\pi x})^2 \tag{1.11}$$

where J_1 corresponds to the first order Bessel function. This is directly related to the notion of contrast. Indeed this criterion corresponds to a contrast between the two maxima of the sum of those functions and the minimum between them, of 26.4% as shown in Figure 1.20. In this thesis, the resolution of the devices I made uses this criterion.

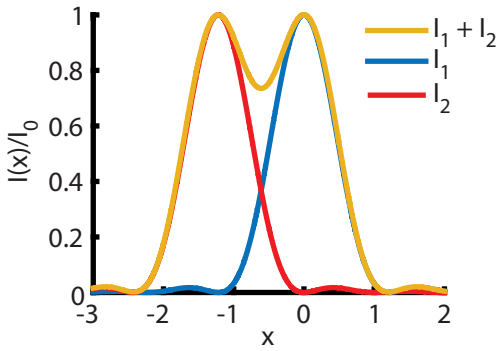

Figure 1.20 – Resolution and contrast. Two Airy functions (red and blue curves) separated by the Rayleigh criterion and their sum (yellow curve). The contrast between the maximum of this sum and the minimum between the two maxima is 26.4%.

Subpixel resolution

The resolution of lensless imaging devices is limited by the pixel size of the camera chip (~several micrometers) and the reconstruction algorithm. Indeed, Claus et al. [89] showed that, since the real resolution limitation comes from the numerical aperture (NA) of the detector subtending the object, it can be taken into account in the reconstruction algorithm

of the holograms to show object details smaller than the detector pixel size. To increase this resolution, several lensless techniques in microscopy have been proposed. Subpixel perspective sweeping microscopy uses images taken at several illumination angles. Between two illumination angles the shadows of the sample move over a subpixel distance. A highly resolved image is then reconstructed numerically. It is particularly interesting for sample with high confluence. A resolution of 660nm with a 2.2μm pixel size over a 24mm^2 field of view has been reported with an on-chip device [52, 90]. However, in this technique, the illumination is on top of the sample which obstructs its view. Another way to increase the resolution is to use optofluidics. X. Cui et al. [91] and G. Zheng et al. [92] used a flow of objects in a microfluidic channel with sub micrometer holes placed along the channel. Several projection images are taken, as the object moves with the flow, with a complementary metal oxide semi-conductor (CMOS) camera of 9.9μm pixel size. A highly resolved image is then reconstructed numerically. A resolution of 750nm has been reported. Finally, in digital inline holography, the increase in resolution has been investigated by using several subpixel shifted holograms on the camera to retrieve a highly resolved hologram that is then processed in a pixel super-resolution algorithm [42, 54, 55, 61, 93, 94]. This technique has been proposed with incoherent illumination to create speckle-free images; however, the compactness of the imager is then compromised since a rather large distance (several centimeters) is needed between the source and the sample to obtain enough spatial coherence. The subpixel shifts are induced by changing either the wavelength of the source by several tens of nanometers [94] or the position of the source on top of the sample as depicted in the examples in Figure 1.19 and in Figure 1.21 [42, 54, 55, 61, 93].

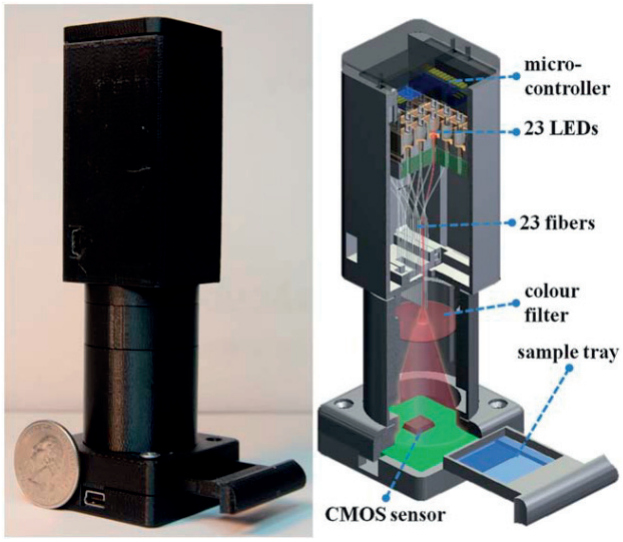

Figure 1.21 – A photograph (left) and a schematic diagram (right) of a lensfree super-resolution microscope (weighing ~95g) are shown. 23 individual multi-mode fiber-optic cables are butt-coupled to 23 LEDs without the use of any lenses or other opto-mechanical components. Using an inexpensive micro-controller, each LED is sequentially turned on and is used as an illumination source to create lensfree holograms of the objects on a CMOS sensor-array. These recorded lensfree holograms are shifted with respect to each other and can be rapidly processed using a pixel super-resolution algorithm. The distance between the fiber end and the sample is about 3-6cm and the sample is placed atop the protective glass of the image sensor ~0.7mm. Reproduced from [61]

2 Compact lensless digital holographic microscopes

In this chapter an in-line and an off-axis compact lensless digital holographic microscopes are presented.
First, the in-line DHM has been developed to obtain a device one order of magnitude smaller in height than other lensless imagers of comparable FOV (see 1.2.1), while providing an unobstructed view of the sample.
The off-axis DHM has then been developed to obtain a device that can be used for high speed imaging because the reconstruction algorithm only requires one digital hologram instead of several for the latter. The device has a FOV one order of magnitude larger that of other off-axis compact DHMs and is more than one order of magnitude more compact (see 1.2.1).

Some of the material presented in this chapter can be found in the following papers:

- M. Rostykus, F. Soulez, M. Unser and C. Moser, "Compact lensless phase imager," Optics Express, vol. 25, no. 4, p. 241, 2017.
- M. Rostykus and C. Moser, "Compact lensless off-axis transmission digital holographic microscope," Optics Express, vol. 25, no. 14, p. 16652, 2017.
- M. Rostykus, F. Soulez, M. Unser and C. Moser, "Compact in-line lensfree digital holographic microscope," Methods, 2017.

2.1 In-line

In-line lensless quantitative phase imaging is of high interest for obtaining a large field of view (FOV), typically the size of the camera chip, to observe biological cell material with high contrast (see 1.2.1). It has the potential to be widely spread due to its inherent simplicity. However, the trade-off is the added complexity of the illumination. Current illumination systems are several centimeters away from the sample, use mechanics to obtain super resolution (i.e., to obtain a spatial resolution smaller than the detector pixel size) or different illumination directions, and block the view to the sample (see 1.2.1). In this section, a side

illumination system which reduces the height by an order of magnitude while providing an unobstructed view of the sample is proposed and demonstrated. This is achieved by shaping the illumination using multiplexed analog holograms that produce 9 illumination angles.
In this section, I elaborated and fabricated the microscopes illumination parts. I set-up the microscopes and I recorded and analyzed the data. I also adjusted the algorithm parameters and ran it. Finally, I also performed the calibration step and processed the data. The phase retrieval algorithm was developed by Dr. Ferréol Soulez from the Biomedical Imaging Group at EPFL.

2.1.1 Device description

Initially, I used a side illuminated waveguide approach for an ultra compact light source. A point source illuminates the waveguide (several millimeters in thickness) which guides light by Total Internal Reflection (TIR). The holographic material is laminated on the bottom side. The TIR is now obtained at the interface between the holographic material and air. An analog grating is recorded between the internally guided light and a collimated beam coming from the top of the waveguide as shown in Figure 2.1. Several attempts were done, however experimentally, the diffraction efficiency and homogeneity of the gratings that I obtained were too low to be usable (diffraction efficiency smaller than 0.01%). A similar geometry for holographic recording was done using a thick photorefractive crystal [95] for data storage and showed good results in efficiency. It might be the mismatch in index of refraction preventing a good coupling of the light in the polymer.

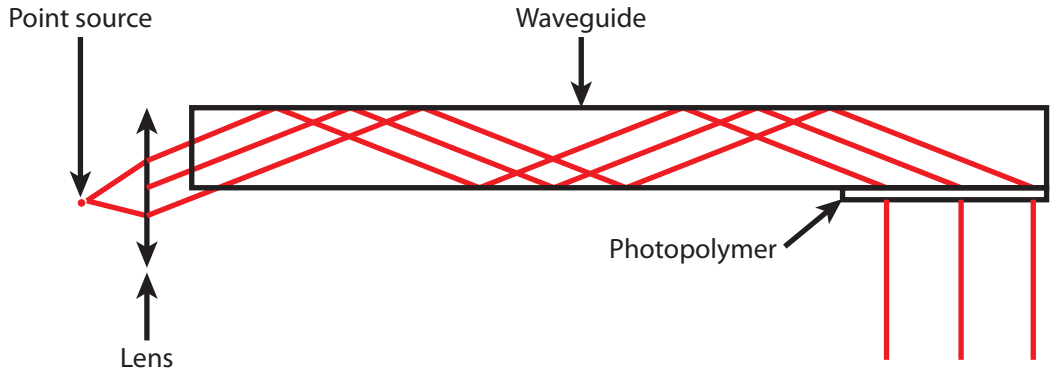

Figure 2.1 – Waveguide device principle scheme.

I switched then to a prism based system instead of a waveguide as Figure 2.2 illustrates.
The illumination is composed of a vertical cavity surface emitting laser (VCSEL, Vixar 680S, single mode, 0.75mW typical output power, 673nm wavelength, 100MHz linewidth) disposed in front of one side of a K9 glass prism. On the opposite side, a BAYFOL®HX photopolymer film of 70μm thickness from Covestro is laminated, as shown in Figure 2.2. The photopolymer is used to record 9 analog hologram gratings to obtain a multi-angle illumination system (see 2.1.2 for more details), in order to be able to retrieve the quantitative phase of the sample

(see 1.1.2). A VCSEL on a translation stage is used as readout source of the hologram gratings. VCSELs are low power consumption lasers (~1mW) which make them suitable for battery operation. It is envisioned that an array of VCSELs can be placed as illustrated in Figure 2.2. For each position of the VCSEL, one diffracted beam illuminates the sample with one illumination direction. It is important to notice that the prism and the photopolymer have similar refractive index to the prism (1.485 vs 1.52 respectively). The beam from the VCSEL is reflected by TIR at the photopolymer-air interface. Indeed, the critical angle at the interface between the photopolymer and the prism is ~80° and the beam's incident angle is ~60° with an angular spread of the VCSEL of ~8°. TIR occurs at the photopolymer-air interface since the critical angle at the interface between the photopolymer and air is ~42°. This ensures that the zero order of the incident beam (i.e. the through undiffracted beam) does not go to the camera which would otherwise create a strong background noise.

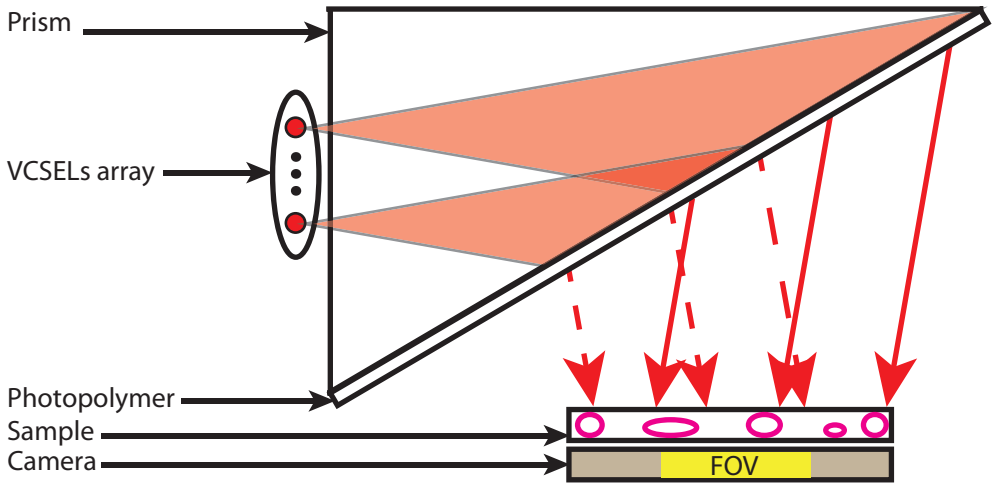

Figure 2.2 – 2D sketch of the compact phase imager with a side illumination system composed of VCSELs illuminating the multiplexed holograms on a photopolymer. For clarity only two angles of illumination out of 9, corresponding to two VCSELs, are shown. All the beams overlap on a ~17mm^2 FOV, corresponding to ~50% of the camera chip size.

Figure 2.3 shows a picture of the device in the laboratory. The camera was tilted and put further away from the prism than during measurements for better visualization on the picture.

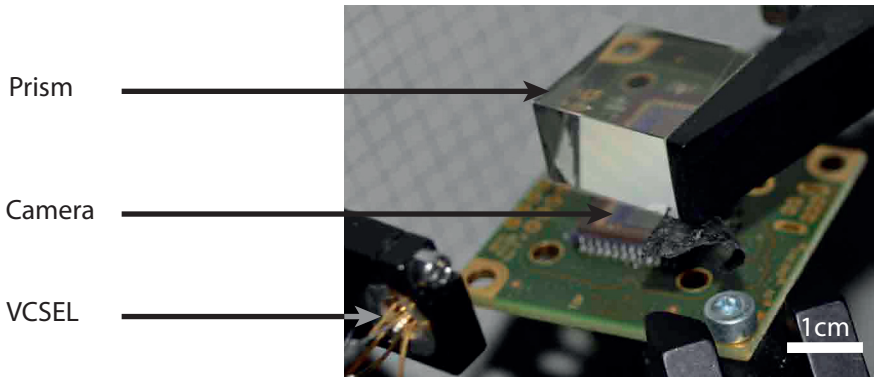

Figure 2.3 – Picture of the device in the laboratory. The camera was tilted and put further away from the prism than during measurements for better visualization on the picture.

2.1.2 Multiplexed gratings fabrication

Nine angularly and spatially multiplexed volume analog holograms are recorded in the photopolymer laminated on the prism. This number was chosen in order to scan the Fourier space in a square shape (see top right inset in Figure 2.6(b)), this is the minimum number.

Recording

For this purpose, a continuous-wave, single frequency red laser (681nm Ondax Compact module) is set in an Mach-Zehnder interferometer configuration (see 1.1.3). The wavefront of the reference beam is chosen to be similar to the wavefront of a VCSEL and the signal beam is collimated. This arrangement is that of the so-called shift multiplexing (see 1.1.3).
In order to obtain several illumination directions, the recording process is sequentially repeated, with each time a spatially shifted position for the reference beam and a different angle for the signal beam, as shown in Figure 2.4. Several hologram gratings are consequently angularly multiplexed in the photopolymer and are addressable by laterally shifting a spherical reference beam. The angle of the signal beam with respect to the normal to the prism is controlled with a 2D galvo mirror system (not shown) (Thorlabs GVS) and the position of the reference beam along the entrance surface of the prism is controlled by a translation stage (Newport CONEX-CC). The signal beam coming from the top is transmitted at the photopolymer-air interface due to the 60 degree prism. Moreover, in order to better control the signal beam direction (to avoid refraction at the output of the prism), a recording prism, with the exact same characteristics of the prism, is added on top of the prism. Index matching oil is added between the two prisms. After recording, the photopolymer is cured using white light having an optical power of approximately 1.8W during 2 minutes in order to fully bleach the absorbing monomers and fix the gratings.

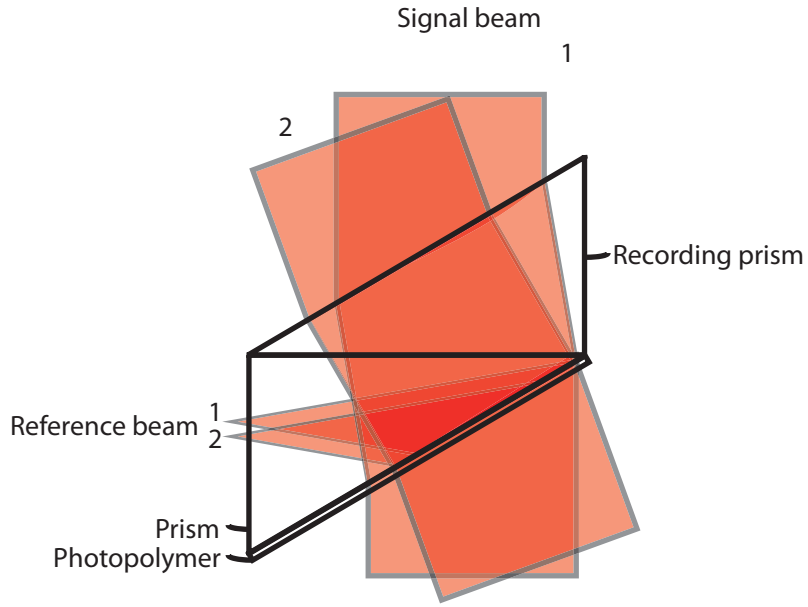

Figure 2.4 – Side view showing multiplexing of two hologram gratings. Reference beam 1 and signal beam 1 interfere in the photopolymer film inducing index of refraction changes, which result in a phase volume grating. The prism is then moved to have the reference beam at position 2 and the signal beam direction is changed to obtain angle 2. The two beams interfere in the photopolymer inducing another phase hologram grating.

The challenge was to obtain similar diffraction efficiencies for all the gratings in order to have the least intensity differences between the different digital holograms and have low crosstalk to avoid superposition of digital holograms on the camera.
As the same diffraction efficiency was wanted for all the different gratings, a similar number of polymerized monomer chains has to contribute to each grating. The beams do not overlap at 100% on the film because of the reference beam shifts that are needed to avoid crosstalk. This means that some parts of the photopolymer are more exposed that others, so less polymerizable monomers are available (see 1.1.3). As the gratings are sequentially recorded in the same area, an exposure schedule had to equalize the diffraction efficiency. Table 2.1 shows the exposure times used for the results of Figure 2.6(b). To obtain this schedule, first, the total exposure time necessary to record one hologram with the highest efficiency was divided by the number of multiplexed holograms. The diffraction efficiencies equalization was then done by trial and error. A precure was performed prior to the recordings (see 1.1.3).

Grating #	1	2	3	4	5	6	7	8	9
Exposure time [ms]	5500	5000	5500	6000	6000	7500	7500	6500	7250

Table 2.1 – Multiplexing exposure times.

Diffraction efficiency

Figure 2.5 shows the setup used to measure the diffraction efficiency and crosstalk of each grating. The prism was displaced in front of the incident laser beam and the optical power of the corresponding diffracted beam is measured with a power-meter. To collect power only from the specific diffracted beam, a collecting lens was placed at a distance such that the other crosstalk beams do not overlap. This measurement was done for each illumination angle, i.e. each grating.

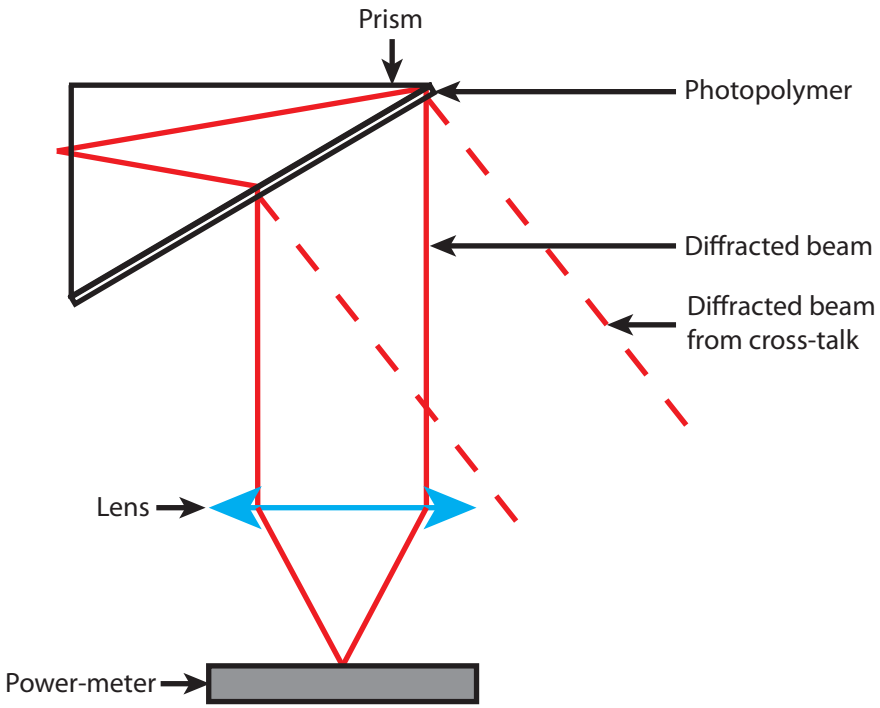

Figure 2.5 – Diffraction efficiency measurements setup. For clarity, only one diffracted angle and one diffracted beam from crosstalk are shown.

Figure 2.6(a) shows the diffraction efficiency of a single phase grating with respect to the in-plane position of the readout point source along the entrance surface of the prism. The peak width gives the shift selectivity. The simulation of the diffraction efficiency as a function of the source position is based on the work of Barbastathis et al. [47] about shift multiplexing with spherical reference waves. The experimental Full Width at Half Maximum (FWHM) is larger than the one of the simulation. The experimental film thickness is smaller than the physical film thickness of 70μm. From the experimental curve, the effective thickness of the holographic film is thus 35μm. This difference can be explained by the fact that the photopolymer layer is quite thick and the gratings are only recorded in the part of the polymer closer to the interface with the glass.

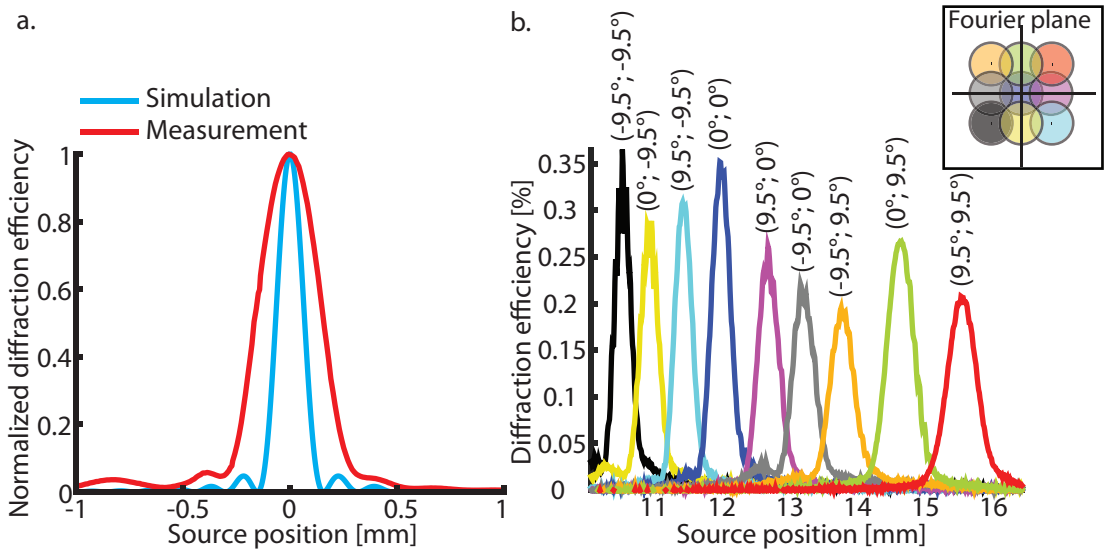

Figure 2.6 – (a) Normalized diffraction efficiency versus source position (ϕ = -11.5°, θ = -11.5°).The experimental curve is broader than what is expected by the theory. This means that the effective thickness of the photopolymer (35µm) is smaller than its physical thickness of 70µm. This behavior has been observed by others when the photopolymer is larger than few tens of micrometers. (b) Diffraction efficiencies of 9 multiplexed hologram gratings versus source position along the entrance surface of the prism.

Figure 2.6(b) represents the diffraction efficiency curves of 9 multiplexed holograms with respect to the in-plane source position along the entrance surface of the prism using the same laser source for recording and readout. When superimposed on the same graph, we can observe that the main contribution of the cross talk (see 1.1.3.) comes from the beam corresponding to adjacent point sources. In the worst case, the relative crosstalk is less than 6% of the main peak, which was found acceptable for the reconstruction algorithm. This is more visible on Figure 2.7.

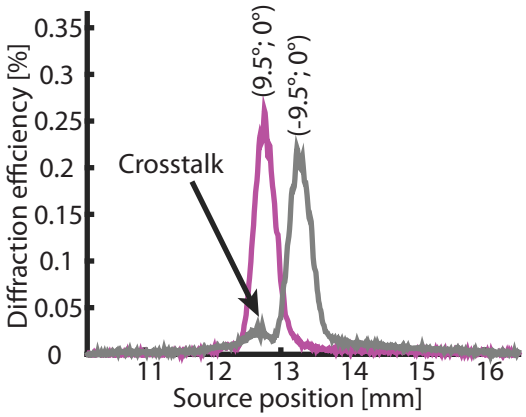

Figure 2.7 – Diffraction efficiencies of 2 multiplexed hologram gratings versus source position along the entrance surface of the prism with crosstalk.

The maximum efficiency measured by recording only one grating on the prism is ~23%. This efficiency is quite low which can be explained by the fact that the two recording beams on the photopolymer were not exactly of the same size. According to the work of Barbastathis et al. [47], the efficiency per grating when multiplexing in such configuration is $(\frac{M_{number}}{M})^2$, where M_{number} is a parameter that depends on the photopolymer and illumination characteristics (wavelength, refractive index change) and M is the number of gratings. For one grating we obtain: $M_{number} = 0.48$. We can then compute the efficiency per grating in the case of 9 gratings: $(\frac{0.48}{9})^2 = 0.28\%$. The efficiency of each peak observed in Figure 2.6 shows a good agreement.

2.1.3 Reconstruction algorithm

One digital in-line hologram was recorded on the camera per illumination angle. A total of nine in-line holograms were thus obtained corresponding to the 9 illumination angles. The amplitude and the phase of the sample are then reconstructed with an algorithm presented below.

Illumination angles estimation

The reconstruction of the phase and amplitude of the sample starts with the estimation of the illumination angles. Indeed, to fit exactly the experiment conditions, the angles are computed from the lateral shifts of the hologram on the camera from the position of the hologram recorded with normal illumination which is taken as the reference. Figure 2.8 shows the case of one illumination direction.

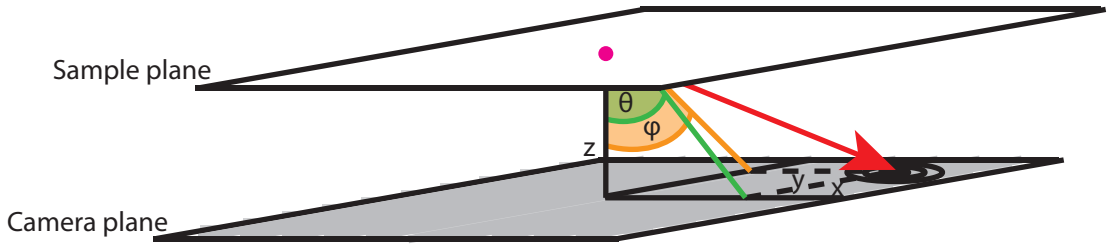

Figure 2.8 – Illumination angles determination. φ and θ are the angles between the normal to the camera plane and the diffracted beam in x and y directions.

The shifts are estimated using a registration algorithm [96]. The algorithm first estimates roughly the shift by crosscorrelation and Fast Fourier Transform (FFT). The steps are:

- Compute the FFT of the two images: FFT_1 and FFT_2
- Do a zero padding of the product $FFT_1 FFT_2^*$, where * means conjugate
- Compute the inverse FFT, which corresponds to an upsampling of the crosscorrelation
- Estimate the shift thanks to the peak location

The estimation of the shift is then refined by upsampling this crosscorrelation in the neighborhood of the first estimation (i.e. of the peak) using Discrete Fourier Transform (DFT). These shifts are then converted in illumination angles using the following equations:

$$\varphi = tan^{-1} \frac{xp}{z} \tag{2.1}$$

$$\theta = tan^{-1} \frac{yp}{z} \tag{2.2}$$

where x (resp.y) is the shift in pixels in one direction (resp. the other one), p is the pixel size and z is the distance between the sample and the camera (see Figure 2.8).

Phase retrieval algorithm

A phase retrieval algorithm then takes the stack of holograms and iteratively estimates the object phase and amplitude with the help of appropriate proximity operators [97]. The reconstructed object $\boldsymbol{o}^+ \in \mathbb{C}^N$ (where N is the number of reconstructed pixels) is estimated in a variational framework by minimizing a cost function which is a sum of the likelihood term $\mathscr{L}$ and a regularization term $\mathscr{R}$:

$$\boldsymbol{o}^+ = \underset{\boldsymbol{o} \in \mathbb{D}^N}{\arg\min}\, \mathscr{L}(\boldsymbol{o}) + \mu \mathscr{R}(\boldsymbol{o}) \ , \tag{2.3}$$

where $\mathbb{D} = \{x \in \mathbb{C}; |x| = 1\}$ is the subspace of $\mathbb{C}$ of phase only objects. μ is a regularization parameter that tunes the balance between the information given by the measurements and the priors. In this approach known as penalized *maximum likelihood*, the data term is defined according to the forward model and the statistics of the noise, whereas the regularization function is designed to enforce some prior knowledge about the object (such as support, non-negativity, smoothness,...). In the presented work, we use the well known total variation regularization function [98]. The equation (2.3) is solved by the mean of the Alternating Direction Method of Multipliers (ADMM). It uses closed form solution or proximity operator of each function [97]. Such an iterative projection method is a Total Variation regularized

evolution of the seminal algorithms of Gerchberg Saxton [99] and Fienup [100].
The main advantages of the proposed algorithm compare to the Gerchberg-Saxton algorithm come from the use of proximity operators [97] and the regularization. First, the algorithm takes Gaussian and Poisson noises into account in the projection step. The field is then extrapolated so diffraction patterns from elements that are not directly seen on the camera are retrieved (the diffraction rings are captured). Finally, higher resolution can be obtained without the use of subpixel shifts, thanks to the different illumination angles. The regularization prevent noise amplification in the phase retrieval process.
The output of the algorithm are the reconstructed amplitude and phase of the sample. In order to obtain quantitative phase results, a calibration of the reconstruction is made using commercial DHM images as references (see Appendix A for more details).

2.1.4 Phase imaging

Dried human epithelial cells on a microscope slide were imaged using the presented device with illumination angles ranging between -9.5° and 9.5° along both directions. The reconstructed phases from the device using 9 holograms and from a commercial DHM (LynceeTec T1003, 5x and 10x objectives) are shown in Figure 2.9. Profile cuts were performed to show the quantitative phase capability of the technique. Using our device, the thickness of the cells can be estimated and is in agreement with the DHM observation. This thickness h is deduced from the phase value using the following equation:

$$h = \frac{\Delta\phi \cdot \lambda}{2\pi\Delta n} \tag{2.4}$$

where, $\Delta\phi$ is the measured phase in radian, λ is the wavelength in vacuum and Δn is the difference between the refractive index of air and that of the dried cell. The refractive index of the dried cell chosen is 1.3. Cells have usually a refractive index comprised between 1.3 and 1.5 depending on their types. The index of refraction is measured with optical techniques based on phase measurement, for example with two different wavelengths in order to decouple the thickness and the refractive index of the cells effects on the phase value [14, 23]. In this thesis, I have not attempted to decouple thickness and refractive index.

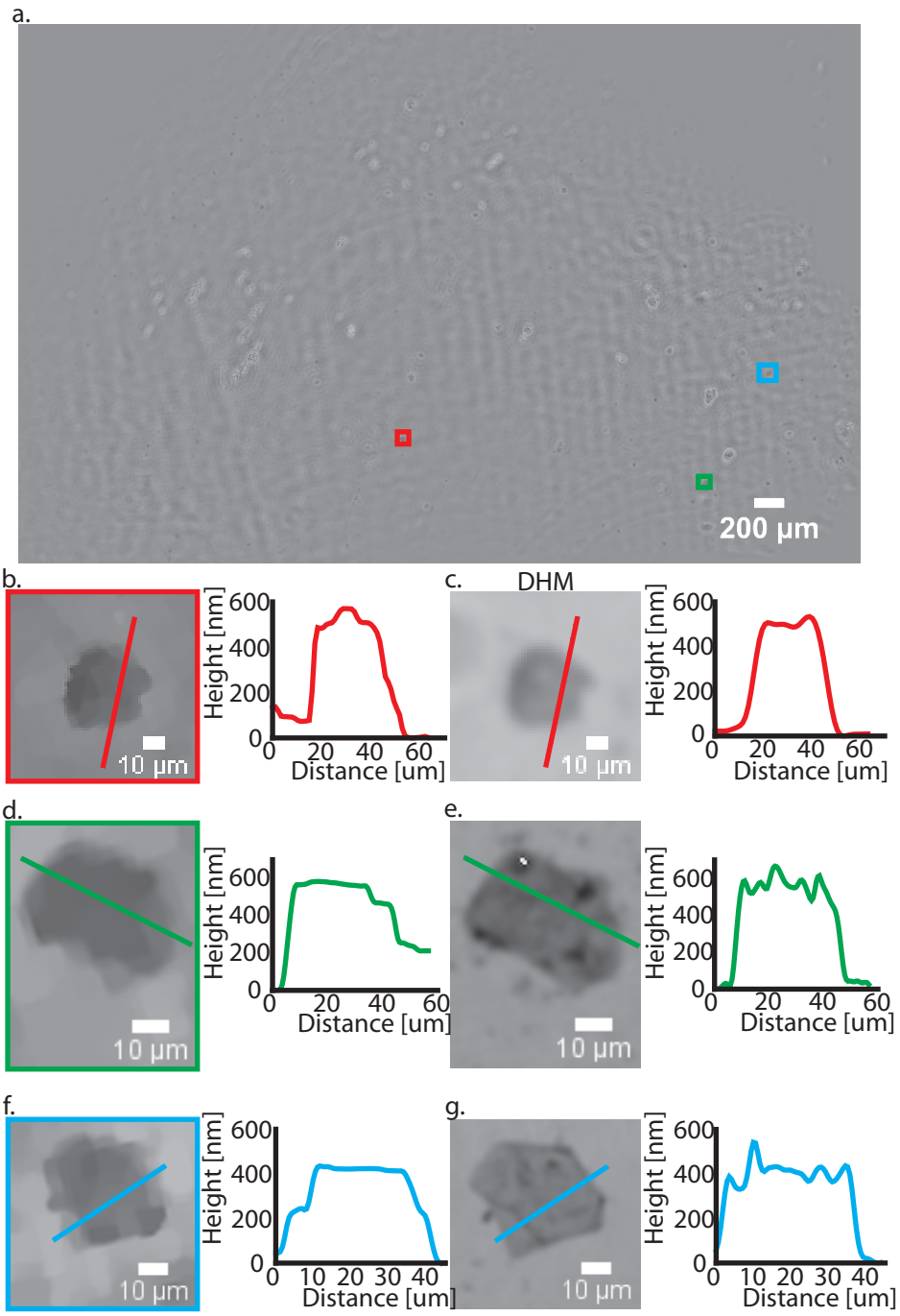

Figure 2.9 – (a) Reconstructed phase with the proposed device and algorithm full FOV. (b) Reconstructed phase with the proposed device and algorithm (crop from a. of 0.0064mm^2). (c) Reconstructed phase with a Digital Holographic Microscope (DHM) using a 5x objective (crop 0.0064 mm^2). (d) Reconstructed phase with the proposed device and algorithm (crop from a. of 0.0033 mm^2). (e) Reconstructed phase with a Digital Holographic Microscope (DHM) using a 10x objective (crop 0.0033 mm^2). (f) Reconstructed phase with the proposed device and algorithm (crop from a. of 0.004 mm^2). (g) Reconstructed phase with a Digital Holographic Microscope (DHM) using a 10x objective (crop 0.004 mm^2).

However, as the illumination with our device is not as uniform as with a DHM, the reconstructed phase image is noisier and shows some 'pixelation' artifacts and non-uniformity across the full FOV. This last point is not a limitation since a calibration is taking into account this non-uniform illumination. The apparent noisy background of the reconstruction is coming from the illumination beams that suffer from non-uniformities originated in the photopolymer substrate, as shown in 1.1.3. Note that the DHM has a FOV about 4 times smaller with a 5x objective for a similar resolution than the proposed method.

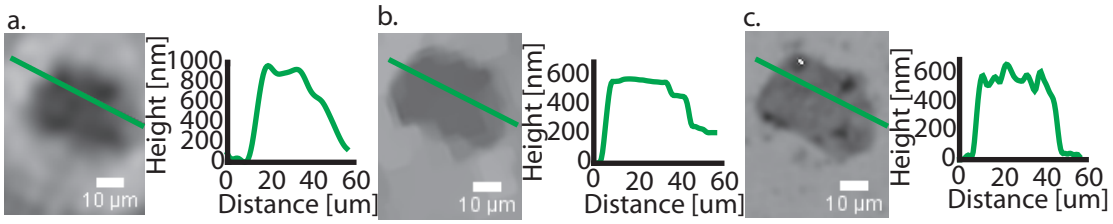

Figure 2.10 – (a) Reconstructed phase by only backpropagating one hologram recorded with the proposed. (b) Reconstructed phase with the proposed device and algorithm. (c) Reconstructed phase with a commercial DHM using a 10x objective.

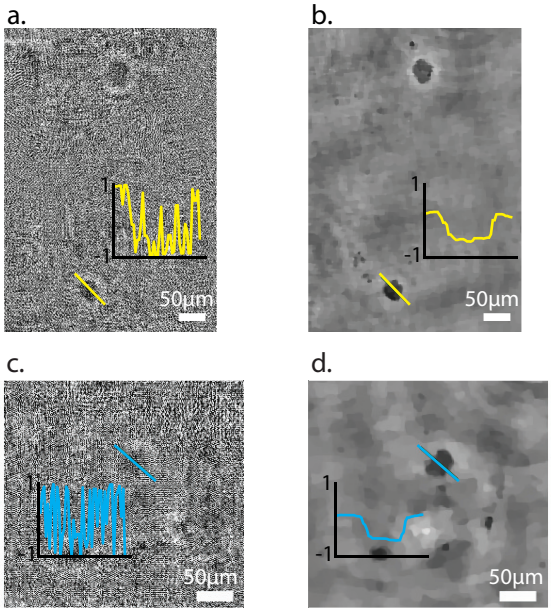

Figure 2.11 – (a) and (c) Reconstructed phase without using regularization. (b) and (d) Reconstructed phase using the proposed regularization.

Figure 2.10 shows the difference between the reconstructed phase by backpropagating only one hologram (Figure 2.10(a)), by using the proposed algorithm with 9 holograms (Figure 2.10(b)) and with a commercial DHM and a 10x objective (Figure 2.10(c)). Since the height of the cell is different from the ground truth image, it is clear that the retrieved phase of the first case is not quantitative. Moreover, Figure 2.11 shows the same reconstructed FOV with

and without the use of the regularization term (see cost function 2.3). The use of the proposed algorithm is thus essential to retrieve a quantitative phase. The morphology of the cells are also better resolved.
The resolution of the proposed device and reconstruction is ~4.92μm, limited by the pixel size [101] and noise. It is important to notice that super resolution is not achieved in the reconstructed images, as depicted in Figure 2.12, likely because of the illumination beam uniformity that is affected by the multiplexing and the noisy photopolymer substrate, as explained in 1.1.3. Figure 2.12(b) has been obtained by illuminating the phase sample directly with the laser beam used to record the multiplexed gratings, which means without going through the prism and diffraction from photopolymer, hence it is a more uniform beam. Digital holograms using the same 9 angles as in Figure 2.12(a) were recorded with the direct beam and reconstructed with the proposed algorithm. This yields better image quality, thus showing that the current image quality obtained with diffraction from the photopolymer can be improved by having a more uniform photopolymer medium.

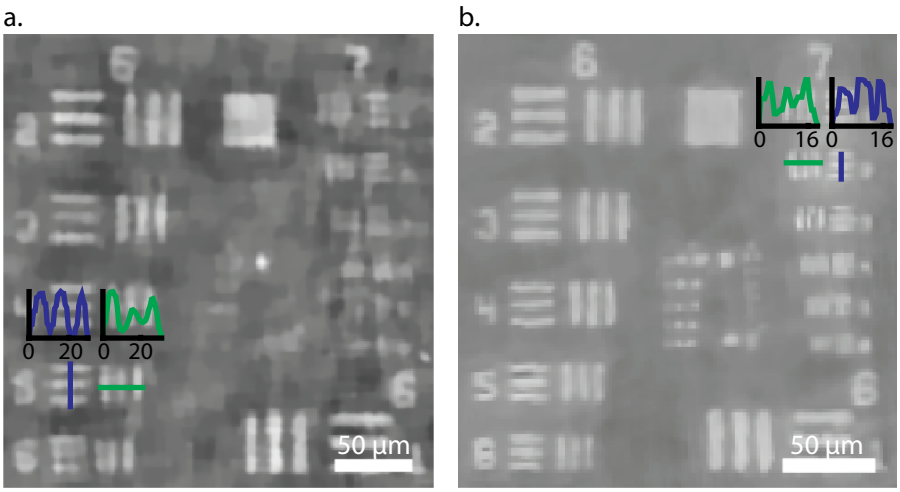

Figure 2.12 – Reconstructed phase of a USAF 1951 phase test target with the proposed device (a) and with direct laser illumination (b). Both reconstructions were performed with the proposed algorithm. A built-in background filtering of ImageJ was applied to (b).

Several representations of in-line holograms obtained by varying the illumination angle are necessary to fully reconstruct, without ambiguity and with high fidelity, the actual quantitative phase of the sample. In addition to the acquisition time, the computing time to perform phase retrieval lengthens the time to obtain a final image. Next I propose a lensless method that is computationally simpler and which requires just a single off-axis hologram to extract the phase image .

2.2 Off-axis

Current compact lensless holographic microscopes are based on either multiple angle in-line holograms (such as the one presented), multiple wavelength illumination or a combination thereof. Complex computational algorithms are necessary to retrieve the phase image which slows down the visualization speed of the image generation, as we just saw. Here, a simple compact lensless transmission holographic microscope is proposed with an off-axis configuration which simplifies considerably the computational processing to visualize the phase images and opens the possibility of real time phase imaging using off the shelf smart phone processors and less than $3 worth of optics and detectors, suitable for broad educational dissemination. This is achieved using a side illumination and analog hologram gratings to shape the reference and signal illumination beams from one light source, as in the previous the section.
In this section, I elaborated and fabricated the microscope illumination parts. I set-up the microscope and I recorded the data. I also ran the reconstruction algorithm and processed the data.

2.2.1 Device description

The illumination is composed of the same prism and VCSEL as the ones in the in-line microscope presented in 2.1. However, two analog volume hologram gratings are recorded separately in the photopolymer at two positions (see 2.2.2 for more details), instead of the 9 angularly and spatially multiplexed gratings. One diffracted beam goes through the sample and the other is used as reference. Both interfere on a camera (The Imaging Source 27UJ003-ML, 1.67μm pixel size, similar to mobile phone camera). The two gratings are designed to diffract the diverging light from the VCSEL inside the prism into two collimated beams separated by a 5.8° angle, as shown in Figure 2.13. The angle between the beams is chosen to respect the Nyquist criterion necessary to resolve the interference fringes on the camera:

$$\sin\theta = \frac{\lambda}{4\text{pix}} \tag{2.5}$$

where θ is the angle between the two beams, pix is the pixel size and λ the wavelength.
During the recording process of a digital hologram, a sample is inserted in one of the two diffracted beams. At ~4cm from the prism, the beams recombine in the camera plane where a digital hologram is recorded. The FOV is 12mm^2.
For ease of use and portability, a box has been designed and 3D printed to contain all the elements of the proposed system. The inset in Figure 2.13 shows a picture of the device in the proposed housing next to a typical smartphone.The box size is: 6.5cmx4.2cmx7cm.

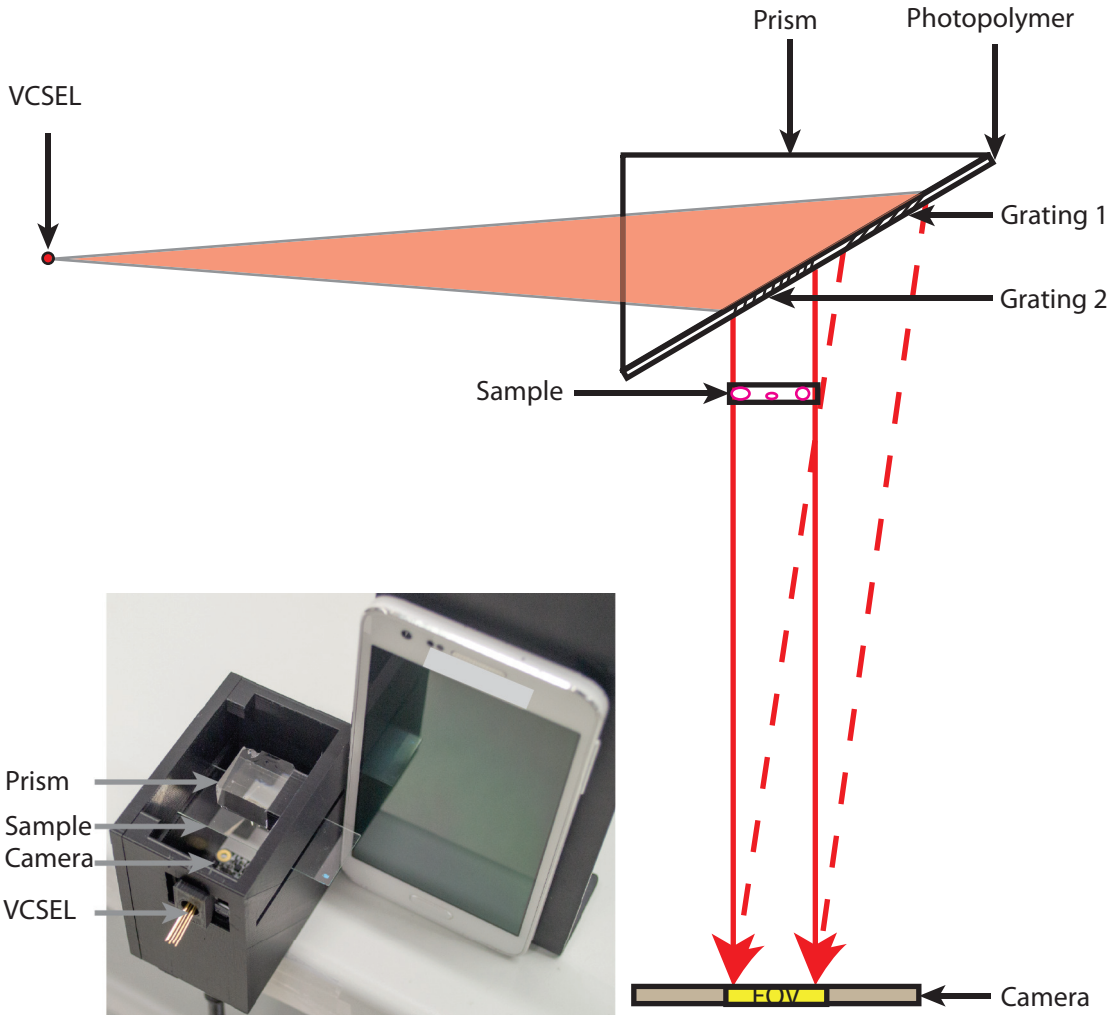

Figure 2.13 – 2D sketch of the compact digital holographic microscope. A VCSEL illuminates two spatially multiplexed volume analog holograms recorded on a photopolymer laminated on a prism. One diffracted beam goes through the sample and the other is used as reference. Both interfere on a camera. The inset is a picture of the device in the proposed 3D printed housing. The smartphone is shown for size comparison.

2.2.2 Multiplexed gratings fabrication

The two spatially multiplexed volume analog holograms are recorded in the photopolymer laminated on the prism. The recording process is similar to that detailed in 2.1.2. The main difference is that the analog holograms are here spatially multiplexed. Only one source/one position of the source in front of the prism is needed in this case since we need to obtain both beams at the same time. The total diffracted light represents ~3.5% of the incident source light. The efficiency is controlled by the exposure time during the gratings recording (see 2.1.2). More efficiency would lead to an over exposition of the camera at the smallest exposure time available.

2.2.3 Reconstruction algorithm

First, a reference digital hologram is recorded without a sample in the beams. The sample is then inserted in one of the two beams and a new digital hologram is recorded. The reference hologram is used to provide a reference phase background of 0 radian to be able to evaluate the quantitative phase of the object. During the reconstruction process, the real or virtual image (see 1.1.2) is selected in the Fourier plane. Amplitude and phase of the sample are then retrieved through backpropagation [17, 32]. The reconstruction process is performed using KOALA software from LynceeTec.

2.2.4 Phase imaging

A digital hologram of a homemade phase 1951 USAF test target (etched soda lime glass) was obtained using the proposed device and the phase and amplitude images were then reconstructed. The hologram, spectrum and phase images are shown in Figure 2.14(a)-(c). For comparison, the same sample was also imaged using a commercial DHM (LynceeTec DHM T1000 Fluo) with a 5x objective and the results are shown in Figure 2.14(d)-(f).

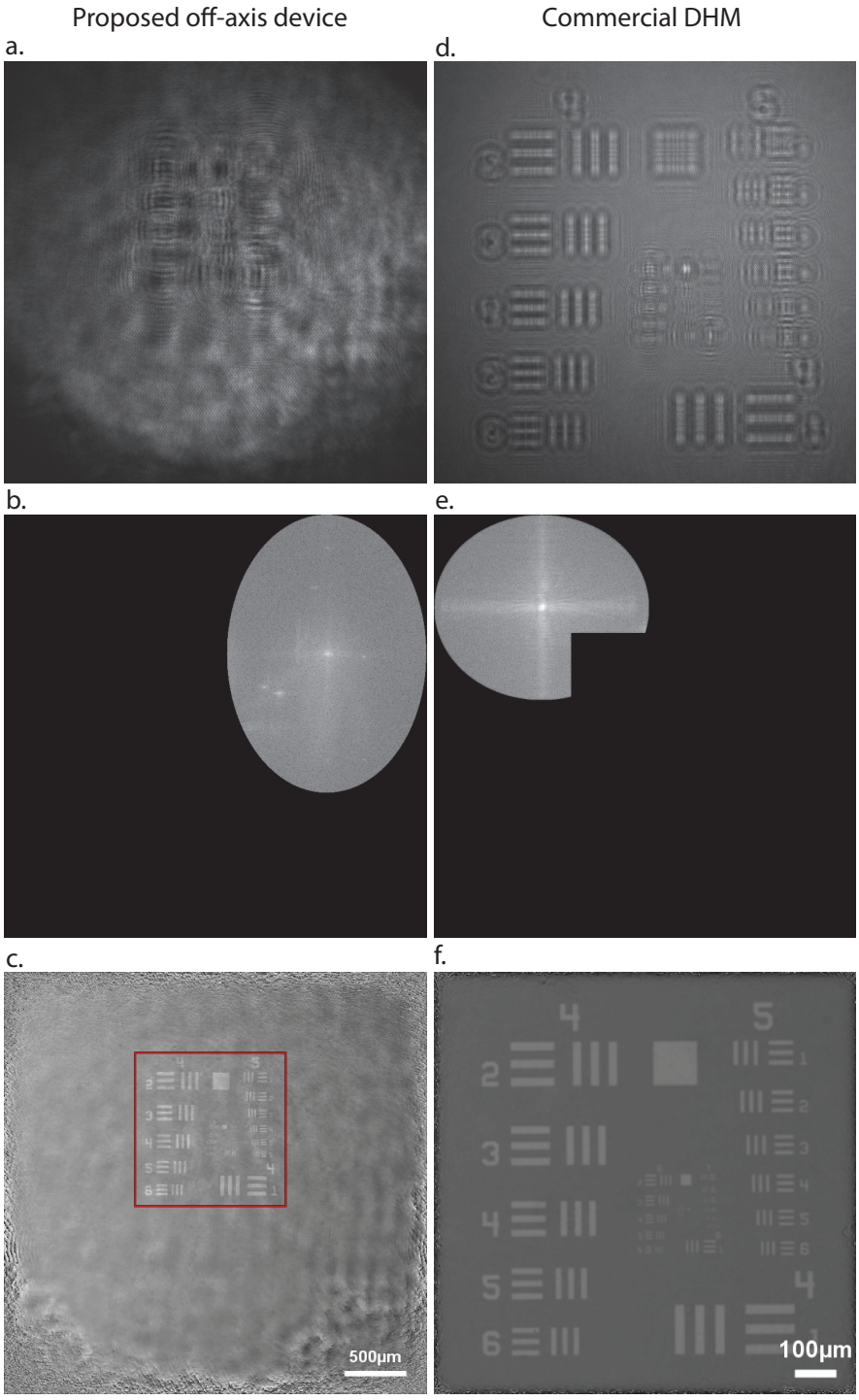

Figure 2.14 – (a) Hologram recorded with the proposed device. (b) Spectrum of hologram (a) with the mask selecting only one image. (c) Reconstructed phase with the proposed device of the full FOV. (d) Hologram recorded with the commercial DHM. (b) Spectrum of hologram (d) with the mask selecting only one image. (f) Reconstructed phase with a commercial DHM (full FOV). The elliptical filtering in (b) is due to the fact that the angles in both directions between the reference and object beams were not equal meaning that the center of the spectrum of the real image is not exactly in the diagonal of the spectrum passing by the DC term.

The etching depth of the sample is measured in the reconstructed phase image with the proposed device and then compared with the phase image obtained with the commercial DHM. The results are shown in Figure 2.15. Excellent quantitative agreement is found. Both measurements show a ~180nm etching depth showing that the proposed device allows obtaining accurate quantitative phase measurements.

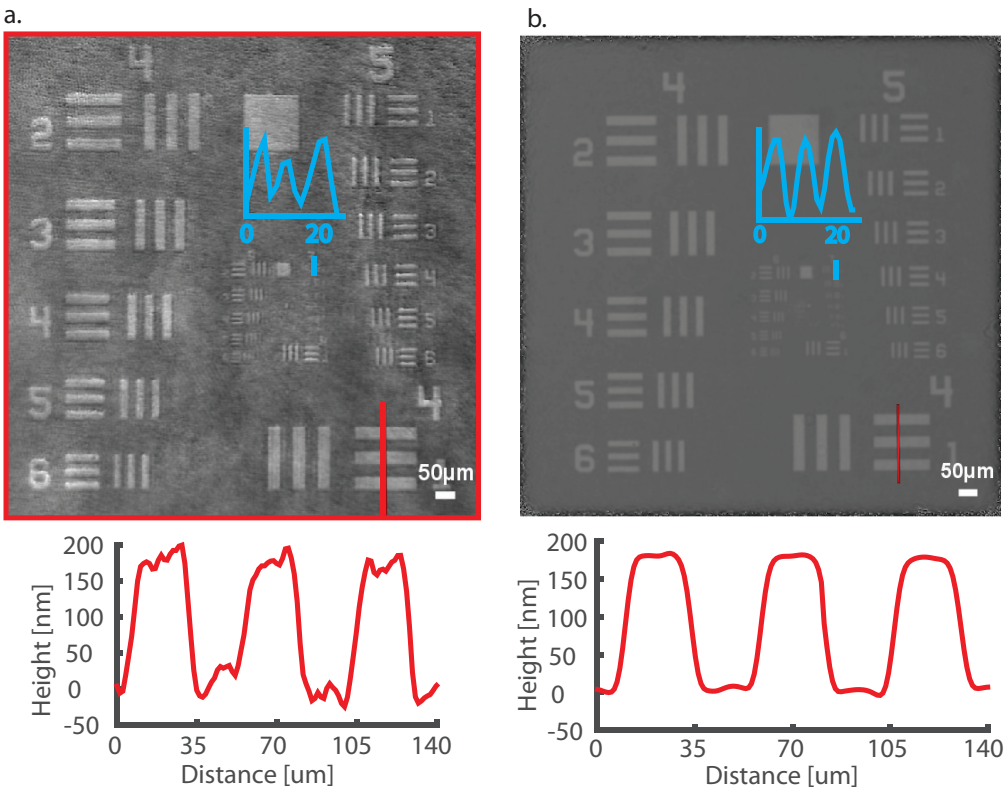

Figure 2.15 – (a) Zoom on the red square of reconstructed phase Figure 2.14(a) (crop of 0.9x0.9mm). (b) Reconstructed phase with a commercial DHM (full FOV).

The temporal noise of the setup was measured by taking the value of the average phase of 5 pixels over the FOV during a time duration of 10 seconds at a frame rate of 6 frames/sec. The presented device has a temporal noise of ~9nm and the commercial DHM ~0.55nm. This noise level can be explained by vibrations in the setup due to the fact that all the elements were not on the same holder. This noise is reduced to 2nm when successive images are taken at the camera rate (6 frames/sec), i.e. when the time between two images is too small to see important vibrations effect. The second origin of the background noise comes from the diffracted beams themselves which are not perfectly spatially uniform in intensity and phase. This is due to the substrate of the photopolymer used to fabricate the gratings (see 1.1.3). Upon lateral vibration, the spatial phase non uniformity translates to phase noise. This background noise can be reduced by using a photopolymer with a cleaner substrate and/or by inserting all the microscope components in the same holder so as to avoid relative vibrations between

them. In this way, a reference hologram of only the reference beam can be used for subtraction. Finally, the noise due to coherence can be removed by digitally filtering the specific unwanted frequencies that can be seen in the spectrum. The lateral resolution obtained with the device is 3.91μm over a FOV of ~12mm^2, which corresponds to ~40% of the camera chip. The resolution is limited by the pixel size and the maximum size of the selected area in the Fourier space during reconstruction. Note that the commercial DHM has a FOV more than 6 times smaller for a resolution of ~3.1μm. A similar experiment was made with dried human epithelial cells on a microscope slide. The result is shown in Figure 2.16(a) along with the reconstruction from a commercial DHM image Figure 2.16(b).

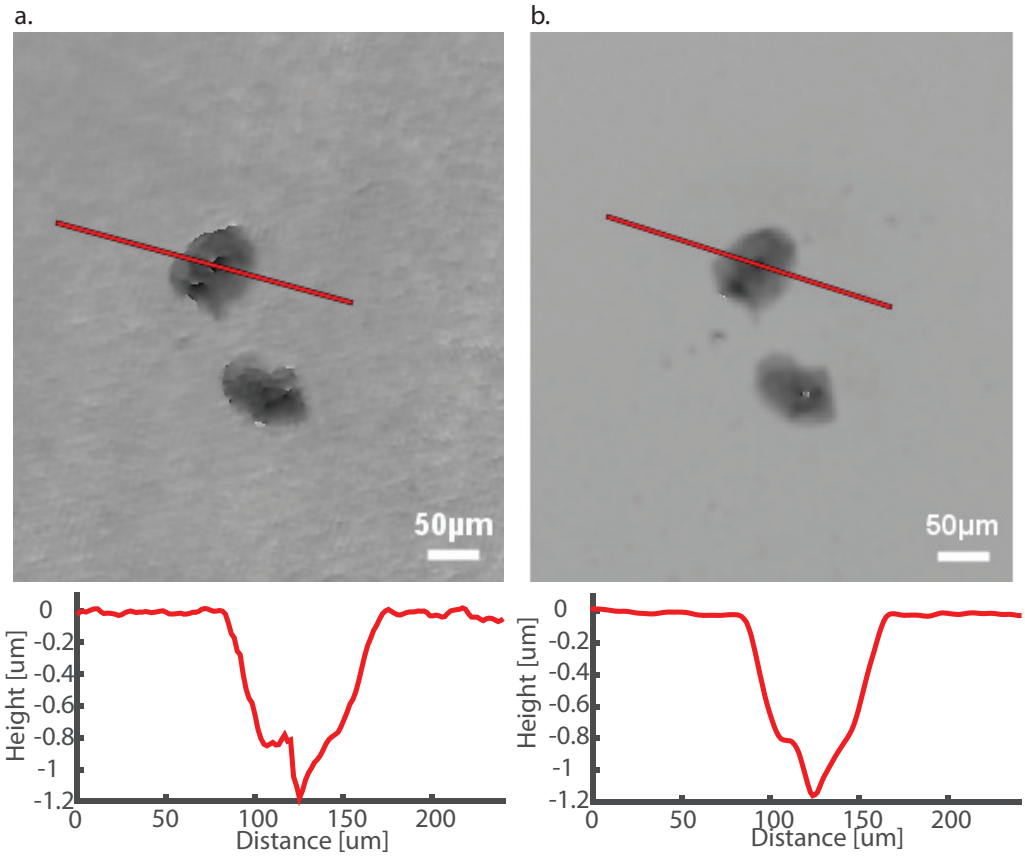

Figure 2.16 – Reconstructed phase of a hologram of human epithelial cells taken with the proposed device (a) and with a commercial DHM (b).

The camera sensor area is larger than the presented FOV. The size of the FOV is related to the size of the diffracted beams from the analog gratings. Indeed, if the size of the diffracted beams is increased, the distance between the two analog gratings must be increased (to have separated beams) which induces a longer distance for the recombination of the two beams, i.e. a less compact device. To have two separated beams and a compact device, the choice was made to have a limited FOV of ~12mm^2, which is already more than 6 times larger than the one obtain with a 5x objective and similar resolution.

3 Compact lensless subpixel resolution large field of view microscope

In this chapter a technique to increase the spatial resolution in a compact lensless digital holographic microscope is presented.

Some of the material presented in this chapter can be found in the following paper:

- M. Rostykus, M. Rossi and C. Moser, "Compact lensless subpixel resolution large field of view microscope," Optics Letters, vol. 43, no. 8, p. 1654, 2018.

A compact digital lensless in-line holographic imager has been developed where subpixel shifts are created by changing the injection current of a VCSEL that illuminates a grating recorded in a photopolymer film. By varying the injection current, the source wavelength changes which in turn changes the diffracted beam angle. The reconstructed resulting image has a lateral resolution smaller than the pixel size.
In this section I elaborated and fabricated the microscope illumination parts. I set-up the microscope and I recorded the data. I also participated to the reconstruction algorithm writing, I ran it and processed the data. Mattia Rossi from the Signal Processing Laboratory (LTS4) at EPFL contributed to the algorithm writing.

3.1 Device description

A compact lensless imager performing phase retrieval has already been presented by the authors [102] but had a resolution limited by the pixel size of the camera . Here, a side illumination system is constructed with a prism onto which a volume phase grating is recorded in a photopolymer (Covestro BAYFOL®HX). The volume hologram is illuminated by a VCSEL (Vixar 680S), which produces a collimated diffracted beam illuminating the sample. Figure 3.1 is a sketch of the device. The employed monochrome camera has a 5.2μm pixel size (Thorlabs DCC1545M).

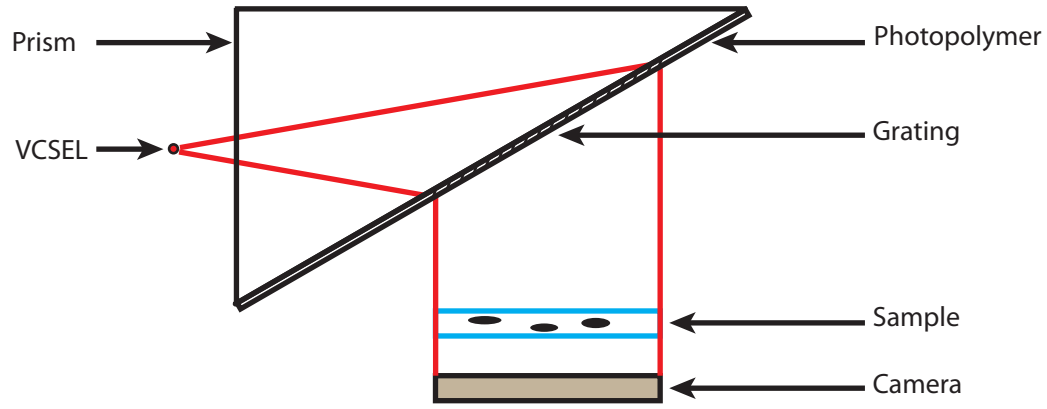

Figure 3.1 – Compact lensless subpixel resolution large field of view microscope sketch.

When the injection current of the light source is changed, it induces a wavelength change of the light. This is shown in Figure 3.2 which shows the wavelength shift with respect to the VCSEL driving current.

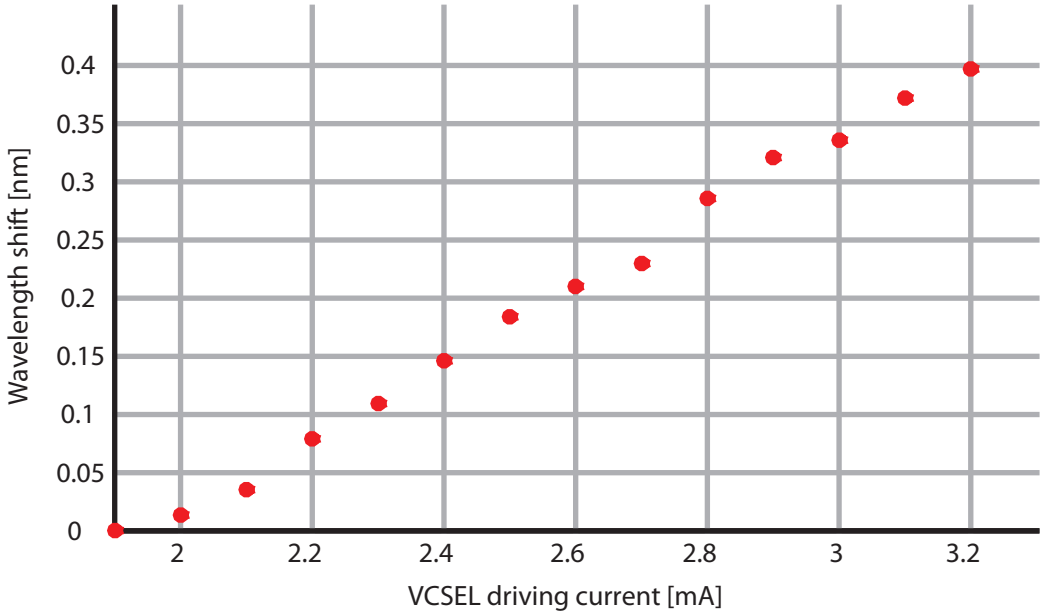

Figure 3.2 – Wavelength shift VS. driving current of the VCSEL.

The change of wavelength results in a slight change in the diffracted angle from the grating. The volume grating has been recorded with a collimated beam and since the wavelength change is very small (0.044%), the diffraction results in a small angular change with negligible deviation from a plane wave. This creates a shift of the hologram on the camera, which depends on the distance between the sample and the camera. Figure 3.3 illustrates this situation. The digital hologram depends also on the wavelength; however since the maximum wavelength change is smaller than 0.5nm, this change is negligible in the reconstruction process.

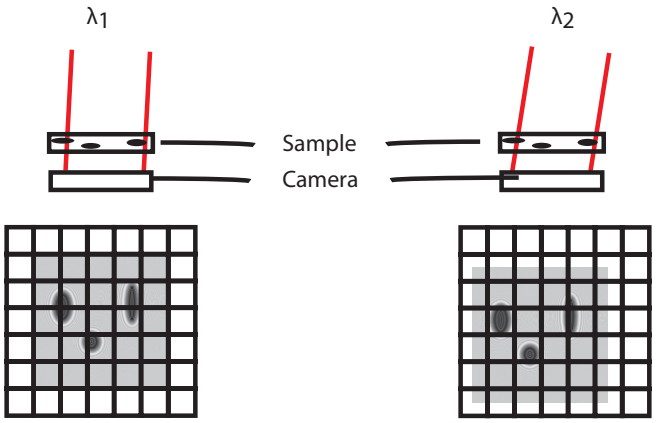

Figure 3.3 – Sketch of the subpixel shift created by the wavelength selective diffraction which changes the illumination angle.

3.2 Grating fabrication

The volume analog hologram is recorded in the photopolymer laminated on the prism. The recording process is the same as the one detailed in 2.1.2. The main difference is that only one grating is recorded. Only one source/one position of the source in front of the prism is needed in this case.

3.3 Reconstruction algorithm

Shifts of all the holograms are estimated [96] using the hologram taken with the lowest driving current as reference. See 2.1.3 for more details. The stack of holograms is then processed in a pixel super-resolution algorithm [103] to reconstruct a highly resolved hologram that is then backpropagated [104].

3.4 Subpixel resolution imaging

In order to obtain shifts in both directions, the camera was tilted compared to the diffraction angle change as depicted in Figure 3.4.

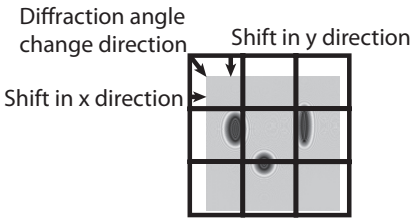

Figure 3.4 – Sketch of the subpixel shifts directions.

Table 3.1 shows the estimated hologram shifts, obtained with the algorithm above, in horizontal and vertical directions at the camera plane with respect to the VCSEL driving current (corresponding to wavelength shifts) for a sample-camera distance of ~7mm. This distance has been chosen to obtain a compact device and to provide a maximum shift of one full pixel at the same time. The change of the illumination angle induces a shift in the Fourier domain; however since the maximum angular shift is ~0.04°, this change is negligible in the reconstruction process.

Shift in x direction [pix]	0	0.06	0.11	0.15	0.17	0.22	0.24	0.25	0.35	0.52
Shift in y direction [pix]	0	-0.1	-0.20	-0.29	-0.34	-0.43	-0.53	-0.65	-0.84	-1.03
VCSEL driving current [mA]	1.9	2	2.1	2.2	2.3	2.4	2.5	2.6	2.7	2.8

Table 3.1 – Hologram shifts for different VCSEL driving currents for a ~7mm sample-camera distance.

10 digital in-line holograms are recorded, corresponding to one per driving current of the VCSEL. A comparison between the resolution of the amplitude reconstructed image obtained with 10 subpixel shifted holograms, and the resolution obtained with 1 hologram taken with a high dynamic range (HDR) is shown in Figure 3.5. The HDR image uses as many holograms as the one reconstructed with the proposed method, which makes the contrast (hence the resolution) comparison more correct. A resolution of ~2.76μm over a FOV of ~28mm^2 is demonstrated using a camera with pixels of 5.2μm. The resolution is improved approximatively by a factor of two. Increasing the number of sub pixel shifted images, would result in higher spatial resolution. Unfortunately, this would also result in a longer acquisition time. Ultimately the improvement in resolution is limited by the numerical aperture (NA) of the detector subtending the object [89] (see 1.2.2) and by intensity noise. In order to mitigate the effect of intensity noise in the image, which comes from the coherent illumination, the introduction of a regularizer, e.g., Total Variation [98], in the current super-resolution algorithm could be used. This method denoises the image without losing spatial resolution. The spatial resolution can be further increased to approach the resolution limit above by taking the pixel function into account and use deconvolution [54]. Indeed, the active area of the pixel is smaller than the pixel and each part of the pixel does not have the same responsivity. The gray scale corresponds to intensity values.

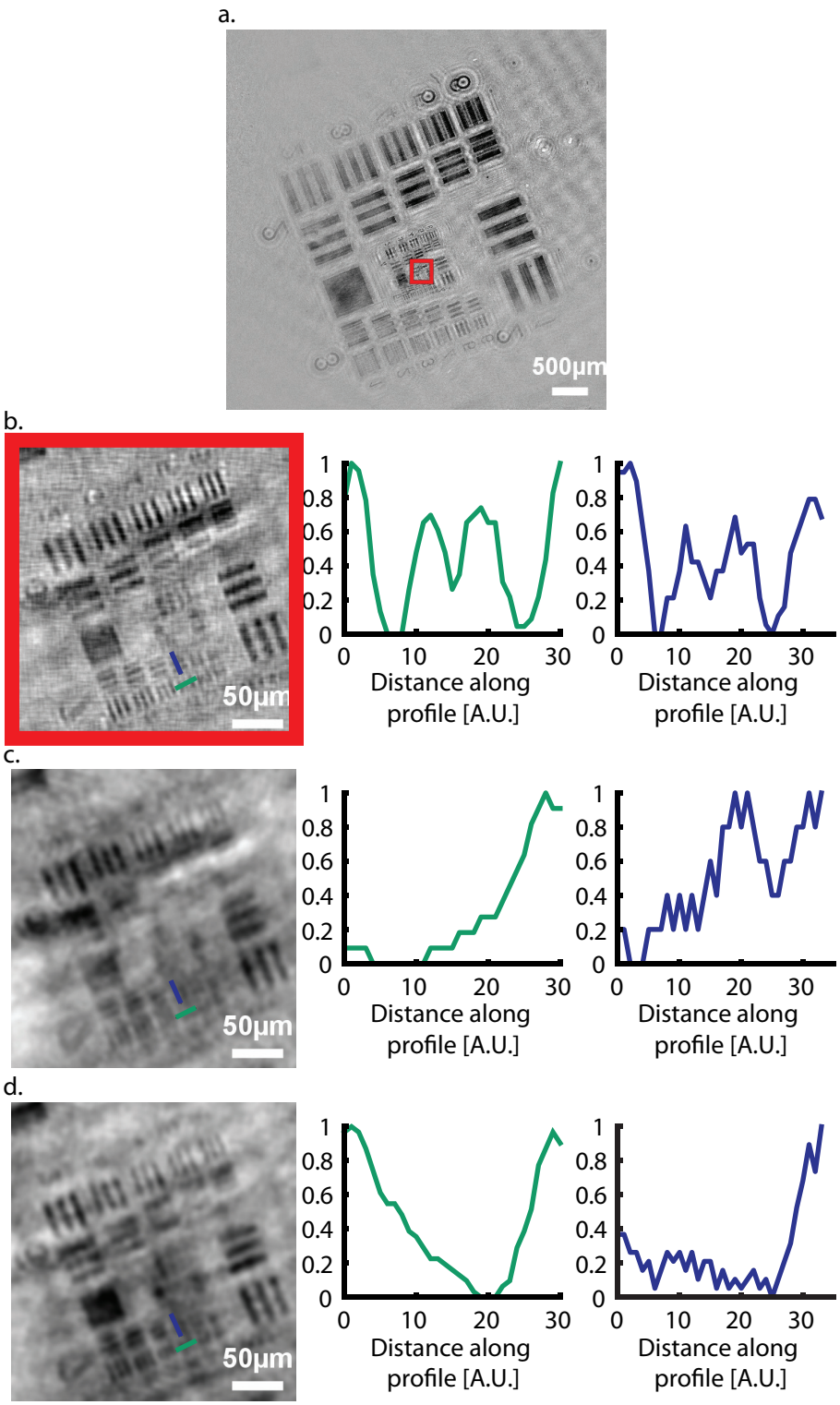

Figure 3.5 – (a) Reconstructed amplitude using 10 holograms (full FOV). (b) Crop of image (a) (crop of ~0.1mm^2). (c) Reconstructed amplitude using 1 hologram (crop of ~0.1mm^2). Reconstructed amplitude from HDR image using 10 holograms with different exposure time (crop of ~0.1mm^2).

The noisy background that can be observed on the reconstructed image comes mainly from two sources. The first one is the non-uniformity of the diffracted beam itself, especially because of the substrate of the photopolymer used to fabricate the gratings (see 1.1.3). The second is the twin image that creates unwanted diffraction patterns around the features. Indeed, in in-line digital holography, the real and virtual images are superimposed with the DC term in the spectrum of the hologram (see 1.1.2). Therefore, one image (real or virtual) cannot be isolated before backpropagation. It is a well-known problem in in-line holography and could be tackled using more image acquisition and processing [34–38, 40, 105]. This is out of the scope of this work, whose objective was to demonstrate pixel super resolution. However, if the presented technique is combined with phase retrieval, the twin image problem can be solved in the phase retrieval process [34, 35, 37, 40].
Two USAF 1951 test targets were superimposed and imaged simultaneously. One was situated at ~7mm from the camera and the second one at ~8mm from the camera. Since the samples are highly absorbing, the smallest features were placed at different location on the camera in x and y directions to avoid overlapping of large absorbing features. Figure 3.6 shows a sketch of the experiment.

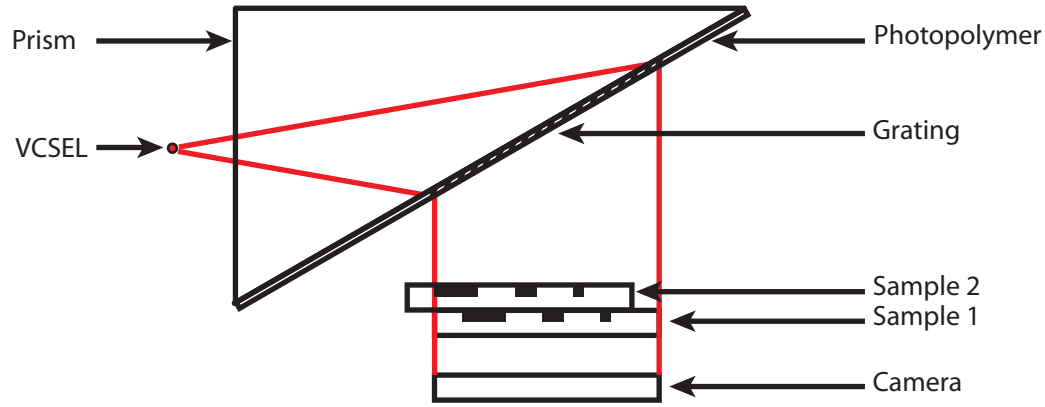

Figure 3.6 – Sketch of the two superimposed sample experiment. Sample 2 is placed on top of sample 1 and its smallest features are placed in order to avoid overlapping with large absorbing features from sample 1.

A comparison between the resolutions of the reconstructed amplitude obtained with 10 subpixel shifted holograms for both depth planes is shown in Figure 3.7. Since the subpixel shifts depend on the distance between the sample and the camera, two sets of shifts were computed, one per object-camera distance. The two reconstructions of the hologram were carried out separately. Finally the reconstructed holograms were propagated with the corresponding object-camera distance.

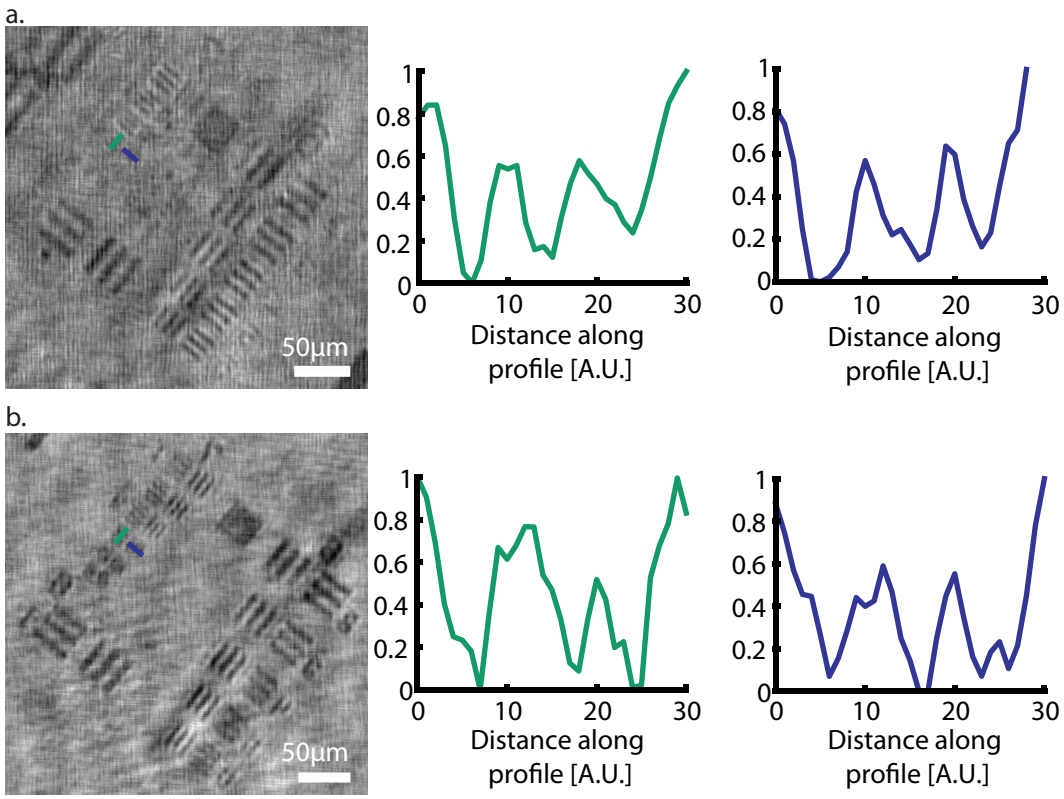

Figure 3.7 – (a) Reconstructed amplitude using 10 holograms of the test target situated at ~7mm from the camera. (b) Reconstructed amplitude using 10 holograms of the test target situated at ~8mm from the camera.

The same resolution is obtained for both targets. This resolution corresponds to the one obtained with the same number of holograms and only one sample between the camera and the prism (see Figure 3.5). It shows that resolution increase can be obtained on at different depths of a sample.

4 Conclusion

In this thesis, three compact lensless digital holographic microscopes and a technique to increase the lateral resolution in lensless compact microscopes were presented.

4.1 Summary of the results

4.1.1 Lensless in-line digital holographic microscope

A side illumination combining VCSELs, a prism and hologram gratings was developed to obtain a 10mm height imaging device, which is almost one order of magnitude shorter than other lensless imagers of comparable FOV. A new phase retrieval algorithm was also implemented allowing the reconstruction of the phase from 9 in-line digital holograms. To demonstrate the phase retrieval ability of the presented device, digital holograms of dried human epithelial cells were recorded. The 9 digital holograms were recorded with 9 different illumination directions obtained by illuminating the device using a VCSEL at 673nm as a readout source for the analog hologram gratings. A phase image of the cells was recovered. To verify that the retrieved phase is quantitative, control phase images from a commercial DHM were taken. The computed heights were similar in both situations, proving the ability of the presented imager to do quantitative phase retrieval. Finally, a resolution of ~4.92μm over a ~17mm^2 FOV was demonstrated.

4.1.2 Lensless off-axis digital holographic microscope

An illumination composed of a VCSEL, a prism and volume hologram gratings was built to obtain a 5cm height quantitative phase microscope, which has a one order of magnitude larger FOV than other off-axis compact DHM and is more than one order of magnitude more compact than other off-axis transmission compact DHM. To demonstrate the phase retrieval ability of the presented device, digital holograms of a 1951 USAF phase test target and dried human epithelial cells were recorded. Phase images of the samples were reconstructed. To verify that the retrieved phase is quantitative, control phase images from a commercial DHM

were taken. The computed heights were similar in both measurements, proving the ability of the presented device to do quantitative phase retrieval. Finally, a resolution of ~3.91μm over a ~12mm^2 FOV was demonstrated. The advantage of the off-axis technique is that only one hologram is required to obtain a quantitative phase. The disadvantage is a less compact design due to the requirement of obtaining an angle.

4.1.3 Subpixel resolution technique for lensless microscope

The presented device offers a large field of view of ~28mm^2 and a resolution of ~2.76μm (4 more groups are resolved compare to a reconstruction with only one hologram on 1951 USAF test target). The increase of resolution is obtained without any mechanical shifts and is using a cheap and efficient light source. This technique could be combined with lensless digital holography design, such as the one presented in this thesis, to also obtain the phase of the sample with high resolution.

4.2 Future work

4.2.1 Lensless in-line digital holographic microscope

Phase retrieval algorithm

In order to reduce the artifacts and increase the phase accuracy of the reconstruction, a new way of estimating the illumination in the phase retrieval algorithm is currently ongoing. Indeed, in the presented results, the illumination was estimated by backpropagating background images. A new approach is to take several background images at different z distances so the complex field can be reconstructed using the same algorithm and used in the phase retrieval process described in 2.1.3. Moreover, work on a new version of the photopolymer is considered which does not have the type of non uniformities encountered in the samples I used in the thesis.

Portable microscope

A VCSELs array is considered to replace the VCSEL on the translation stage in order to obtain a hand-held version of the microscope without any mechanics. Each VCSEL will be switched on one after another, which will correspond to one illumination direction at a time. The integration of all the components in a 3D printed box is ongoing with a user interface addressing the different VCSELs and synchronizing with the image capture.

New illumination source

The company L.E.S.S. SA proposes a ring-shape illumination source based on a side illumination that could replace the prism in this project. The ring shape allows to have the different illumination directions needed and a more uniform illumination. However, as the light from this device is broadband (white light) and incoherent, spatial filter and spectral filter will be added between the ring light source and the sample in order to obtain enough spatial coherence to create a digital hologram and wavelength diversity which helps in the reconstruction. Figure 4.1 shows a sketch of the system.

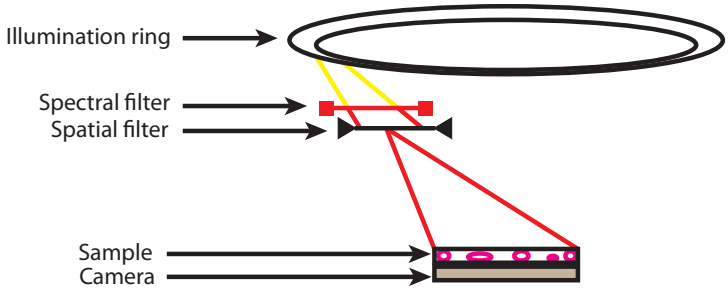

Figure 4.1 – Sketch of the proposed compact lensless in-line digital holographic microscope using a ring light source.

Multi-modal imaging

The presented microscope has a free visual access to the sample from the top which allows for different imaging modalities at the same time, for example fluorescence imaging as depicted in Figure 4.2.

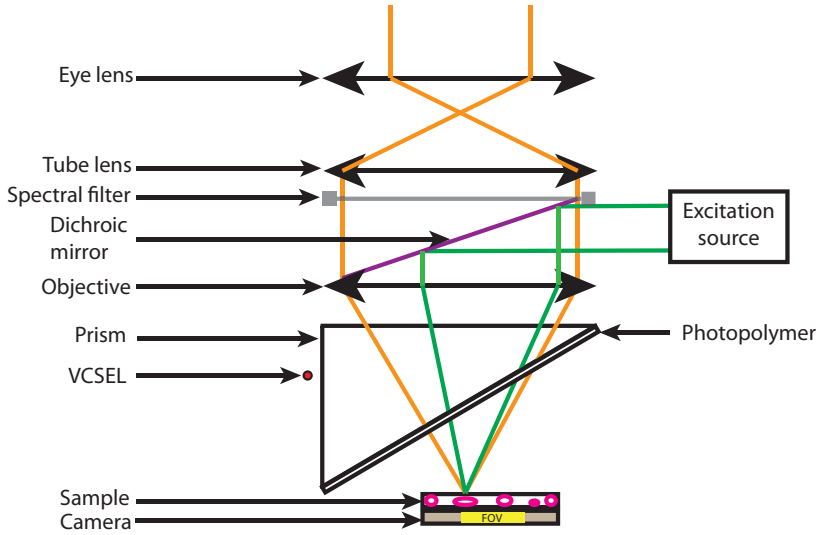

Figure 4.2 – Sketch of the proposed fluorescence compact lensless in-line digital holographic microscope.

4.2.2 Lensless off-axis digital holographic microscope

Resolution

A super-resolution version using the presented subpixel resolution technique is in progress. In order to obtain a higher resolution, the angle between the two beams can be chosen to obtain interference fringes smaller than the pixel size of the camera (larger angle). By using the subpixel resolution technique, those fringes could be retrieved leading to an increase of resolution and a more compact device. Another idea would be to multiplexed hologram gratings, as in the presented in-line microscope but this time to obtain several off-axis digital holograms. This would lead to the scanning of the Fourier space, hence an increase of resolution. This was demonstrated by Dardikman et al. in [106].

Quasi-live imaging

Interfacing the device with KOALA software from LynceeTec is considered in order to be able to see cellular processes, such as cellular differentiation, in quasi-live.

Multi-modal imaging

The presented off-axis DHM also has a free visual access to the sample from the top which allows for different imaging modalities at the same time, such as photothermal imaging demonstrated by Turko et al. [107].

4.2.3 Subpixel resolution technique for lensless microscope

Pixel super-resolution algorithm

The presented results were obtained using a pixel super-resolution algorithm that does not include regularization. A new algorithm developed by Fournier et al. [108] that contains a regularization step could be used to obtain results with less artifacts.

Quantitative phase imaging

The presented subpixel resolution technique combined with digital holographic microscopy is in progress.

Dezoom

Perraut et al. [109] demonstrated a magnification smaller than 1 in lensless microscopy by using a convergent illumination beam. This could be applied to the proposed device in order to increase its FOV as depicted in Figure 4.3. The technique to increase the resolution could

then be applied to obtain an ultra large FOV with subpixel resolution.

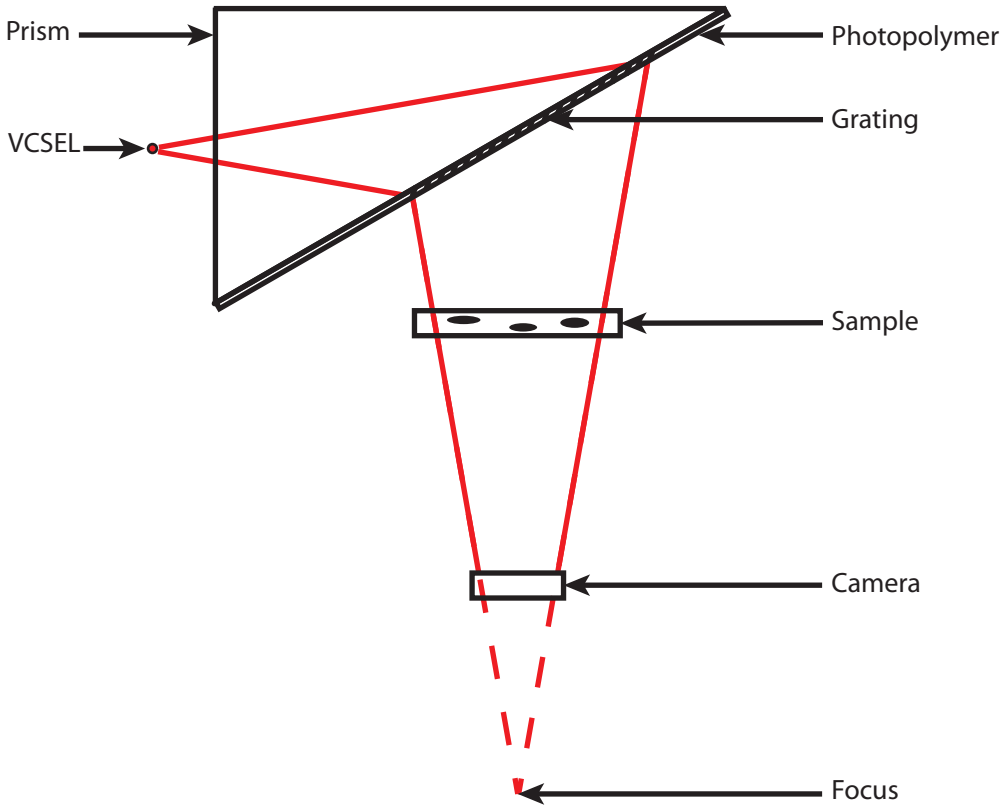

Figure 4.3 – Compact lensless ultra large field of view subpixel resolution microscope sketch. The converging incident beam allows a magnification smaller than 1, hence an ultra large FOV.

A Phase calibration for the in-line microscope

To obtain a quantitative value of the reconstructed phase of the sample a calibration is necessary. That was done by imaging dried human epithelial cells on microscope slides using a commercial DHM from LynceeTec and the proposed in-line microscope. In order to compare the thickness of the cells from both results and obtain a calibration curve, an image registration plugin for ImageJ, Turboreg [110], was used to compare the exact same profile cuts from the commercial DHM and the proposed device reconstructed phases. Figure A.1 shows the calibration curves obtained.

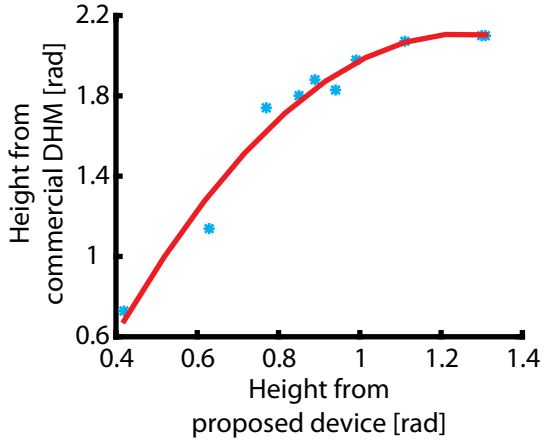

Figure A.1 – Calibration curve. Blue stars: measurements. Red: fitting curve.

The fitting curve is given by the following quadratic polynomial:

$$f(x) = -2.0488x^2 + 5.1445x - 1.1197 \tag{A.1}$$

with a Root Mean Squared Error (RMSE) of 0.78 and a coefficient of determination (R^2) of 0.79. In order to check the validity of the calibration, cells in two different field of view of the same sample were imaged and compared with DHM measurements. The reconstructed phase along with profile plot are shown in Figure A.2.

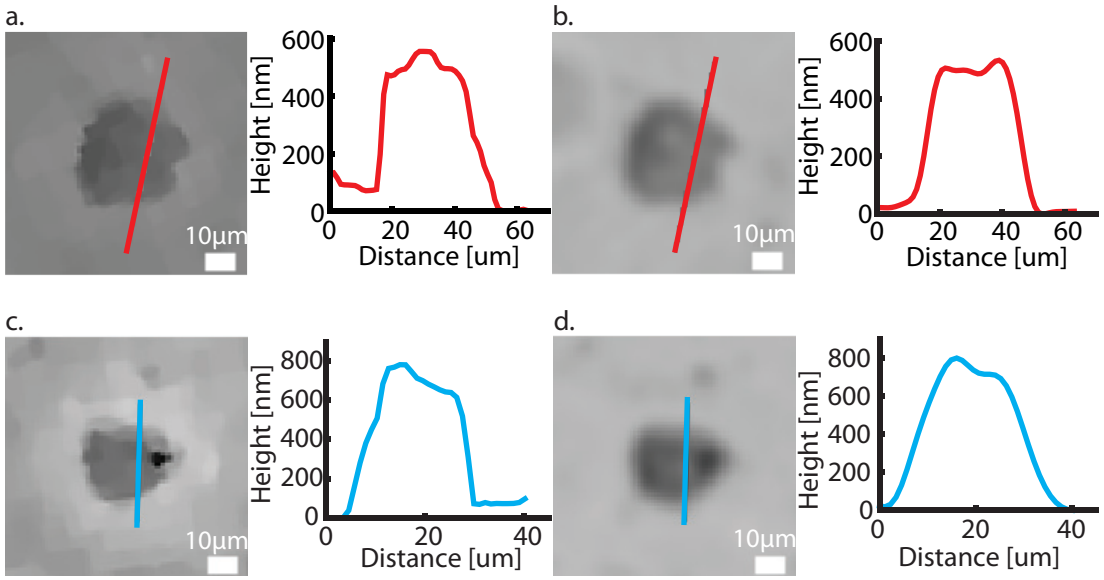

Figure A.2 – (a) and (c) Reconstructed phase with the proposed method from two different field of views. (b) and (d) are the corresponding reconstructed phase from commercial DHM and 5x objective.

Results from measurements of cells from another sample are represented in Figure A.3.

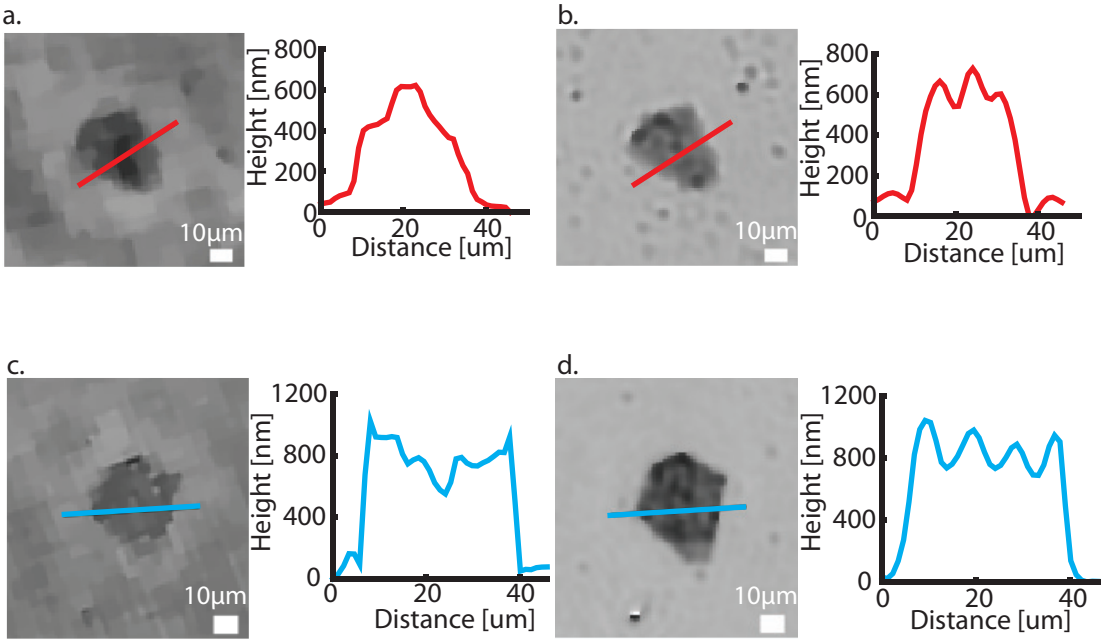

Figure A.3 – (a) and (c) Reconstructed phase with the proposed method from two different samples. (b) and (d) are the corresponding reconstructed phase from commercial DHM and 5x objective.

Some halos are visible around some cells. They are due to a noisy estimation of low frequencies phase. Indeed, in-line holograms of phase objects cannot capture low frequency phase information. This effect is also present in transport of intensity experiments that share similar experimental conditions (i.e. sample-camera distance < 900μm) [111, 112] and other quantitative phase imaging techniques [113, 114]. This can affect the results.

Bibliography

[1] F. Zernike, "Phase contrast, a new method for the microscopic observation of transparent objects part II," *Physica*, vol. 9, no. 10, pp. 974–986, 1942.

[2] M. Wolman, "Polarized light microscopy as a tool of diagnostic pathology.," *Journal of Histochemistry & Cytochemistry*, vol. 23, pp. 21–50, 1 1975.

[3] D. B. Murphy and M. W. Davidson, *Fundamentals of Light Microscopy and Electronic Imaging*. Hoboken, NJ, USA: John Wiley & Sons, Inc., wiley-blac ed., 9 2012.

[4] E. D. Salmon and R. R. Segall, "Calcium-labile mitotic spindles isolated from sea urchin eggs (lytechinus variegatus)," *Journal of Cell Biology*, vol. 86, no. 2, pp. 355–365, 1980.

[5] L. Tian and L. Waller, "3D intensity and phase imaging from light field measurements in an LED array microscope," *Optica*, vol. 2, no. 2, p. 104, 2015.

[6] M. R. Teague, "Deterministic phase retrieval: a Green's function solution," *Journal of the Optical Society of America*, vol. 73, no. 11, p. 1434, 1983.

[7] T. E. Gureyev, A. Roberts, and K. A. Nugent, "Partially coherent fields, the transport-of-intensity equation, and phase uniqueness," *Journal of the Optical Society of America A*, vol. 12, p. 1942, 9 1995.

[8] J. Primot, "Three-wave lateral shearing interferometer.," *Applied optics*, vol. 32, pp. 6242–6249, 1993.

[9] P. Bon, G. Maucort, B. Wattellier, and S. Monneret, "Quadriwave lateral shearing interferometry for quantitative phase microscopy of living cells," *Optics Express*, vol. 17, p. 13080, 7 2009.

[10] G. Di Caprio, M. A. Gioffrè, N. Saffioti, S. Grilli, P. Ferraro, R. Puglisi, D. Balduzzi, A. Galli, and G. Coppola, "Quantitative label-free animal sperm imaging by means of digital holographic microscopy," *IEEE Journal on Selected Topics in Quantum Electronics*, vol. 16, no. 4, pp. 833–840, 2010.

[11] I. Bernhardt, L. Ivanova, P. Langehanenberg, B. Kemper, and G. von Bally, "Application of digital holographic microscopy to investigate the sedimentation of intact red blood

cells and their interaction with artificial surfaces," *Bioelectrochemistry*, vol. 73, no. 2, pp. 92–96, 2008.

[12] N. Pavillon, A. Benke, D. Boss, C. Moratal, J. Kühn, P. Jourdain, C. Depeursinge, P. J. Magistrettiy, and P. Marquety, "Cell morphology and intracellular ionic homeostasis explored with a multimodal approach combining epifluorescence and digital holographic microscopy," *Journal of Biophotonics*, vol. 3, no. 7, pp. 432–436, 2010.

[13] B. Rappaz, A. Barbul, Y. Emery, R. Korenstein, C. Depeursinge, P. J. Magistretti, and P. Marquet, "Comparative study of human erythrocytes by digital holographic microscopy, confocal microscopy, and impedance volume analyzer," *Cytometry Part A*, vol. 73, no. 10, pp. 895–903, 2008.

[14] B. Rappaz, P. Marquet, E. Cuche, Y. Emery, C. Depeursinge, and P. J. Magistretti, "Measurement of the integral refractive index and dynamic cell morphometry of living cells with digital holographic microscopy," *Optics Express*, vol. 13, no. 23, p. 9361, 2005.

[15] K. J. Chalut, A. E. Ekpenyong, W. L. Clegg, I. C. Melhuish, and J. Guck, "Quantifying cellular differentiation by physical phenotype using digital holographic microscopy," *Integrative Biology*, vol. 4, no. 3, p. 280, 2012.

[16] M. K. Kim, "Principles and techniques of digital holographic microscopy," *SPIE Reviews*, vol. 1, no. 1, p. 018005, 2010.

[17] U. Schnars and W. Jueptner, *Digital Holography*. Berlin/Heidelberg: Springer-Verlag, 2005.

[18] J. Kühn, E. Shaffer, J. Mena, B. Breton, J. Parent, B. Rappaz, M. Chambon, Y. Emery, P. Magistretti, C. Depeursinge, P. Marquet, and G. Turcatti, "Label-Free Cytotoxicity Screening Assay by Digital Holographic Microscopy," *ASSAY and Drug Development Technologies*, vol. 11, no. 2, pp. 101–107, 2013.

[19] L. Yu, S. Mohanty, J. Zhang, S. Genc, M. K. Kim, M. W. Berns, and Z. Chen, "Digital holographic microscopy for quantitative cell dynamic evaluation during laser microsurgery," *Optics Express*, vol. 17, p. 12031, 7 2009.

[20] B. Kemper, A. Bauwens, A. Vollmer, S. Ketelhut, P. Langehanenberg, J. Müthing, H. Karch, and G. von Bally, "Label-free quantitative cell division monitoring of endothelial cells by digital holographic microscopy," *Journal of biomedical optics*, vol. 15, no. 3, p. 036009, 2010.

[21] A. Khmaladze, R. L. Matz, T. Epstein, J. Jasensky, M. M. Banaszak Holl, and Z. Chen, "Cell volume changes during apoptosis monitored in real time using digital holographic microscopy," *Journal of Structural Biology*, vol. 178, no. 3, pp. 270–278, 2012.

[22] D. Boss, J. Kühn, P. Jourdain, C. Depeursinge, P. J. Magistretti, and P. Marquet, "Measurement of absolute cell volume, osmotic membrane water permeability, and refractive

index of transmembrane water and solute flux by digital holographic microscopy," *Journal of Biomedical Optics*, vol. 18, no. 3, p. 036007, 2013.

[23] B. Rappaz, F. Charrière, C. Depeursinge, P. J. Magistretti, and P. Marquet, "Simultaneous cell morphometry and refractive index measurement with dual-wavelength digital holographic microscopy and dye-enhanced dispersion of perfusion medium," *Optics Letters*, vol. 33, no. 7, p. 744, 2008.

[24] N. Pavillon, J. Kühn, C. Moratal, P. Jourdain, C. Depeursinge, P. J. Magistretti, and P. Marquet, "Early cell death detection with digital holographic microscopy," *PLoS ONE*, vol. 7, no. 1, pp. 1–9, 2012.

[25] J. Sheng, E. Malkiel, J. Katz, J. Adolf, R. Belas, and A. R. Place, "Digital holographic microscopy reveals prey-induced changes in swimming behavior of predatory dinoflagellates," *Proceedings of the National Academy of Sciences*, vol. 104, no. 44, pp. 17512–17517, 2007.

[26] A. El Mallahi, C. Minetti, and F. Dubois, "Automated three-dimensional detection and classification of living organisms using digital holographic microscopy with partial spatial coherent source: application to the monitoring of drinking water resources," *Applied Optics*, vol. 52, no. 1, p. A68, 2013.

[27] S. K. Jericho, P. Klages, J. Nadeau, E. M. Dumas, M. H. Jericho, and H. J. Kreuzer, "In-line digital holographic microscopy for terrestrial and exobiological research," *Planetary and Space Science*, vol. 58, no. 4, pp. 701–705, 2010.

[28] C. J. Mann, L. Yu, and M. K. Kim, "Movies of cellular and sub-cellular motion by digital holographic microscopy.," *Biomedical engineering online*, vol. 5, p. 21, 2006.

[29] M. Heydt, M. E. Pettitt, X. Cao, M. E. Callow, J. A. Callow, M. Grunze, and A. Rosenhahn, "Settlement behavior of zoospores of Ulva linza during surface selection studied by digital holographic microscopy," *Biointerphases*, vol. 7, no. 1-4, pp. 1–7, 2012.

[30] P. Marquet, C. Depeursinge, and P. J. Magistretti, "Review of quantitative phase-digital holographic microscopy: promising novel imaging technique to resolve neuronal network activity and identify cellular biomarkers of psychiatric disorders," *Neurophotonics*, vol. 1, no. 2, p. 020901, 2014.

[31] R. Barer, "Determination of Dry Mass, Thickness, Solid and Water Concentration in Living Cells," *Nature*, vol. 172, pp. 1097–1098, 12 1953.

[32] U. Schnars and W. Jüptner, "Direct recording of holograms by a CCD target and numerical reconstruction.," *Applied optics*, vol. 33, pp. 179–81, 1 1994.

[33] E. Cuche, P. Marquet, and C. Depeursinge, "Simultaneous amplitude-contrast and quantitative phase-contrast microscopy by numerical reconstruction of Fresnel off-axis holograms.," *Applied optics*, vol. 38, no. 34, pp. 6994–7001, 1999.

[34] G. Koren, F. Polack, and D. Joyeux, "Iterative algorithms for twin-image elimination in in-line holography using finite-support constraints," *Journal of the Optical Society of America A*, vol. 10, no. 3, pp. 423–433, 1993.

[35] G. Liu and P. D. Scott, "Phase retrieval and twin-image elimination for in-line Fresnel holograms," *Journal of the Optical Society of America A*, vol. 4, p. 159, 1 1987.

[36] T. Latychevskaia and H.-W. Fink, "Solution to the Twin Image Problem in Holography," *Physical Review Letters*, vol. 98, no. 23, p. 233901, 2007.

[37] B. M. Hennelly, D. P. Kelly, N. Pandey, and D. Monaghan, "Review of Twin Reduction and Twin Removal Techniques in Holography," in *China-Ireland information and communications technologies conference.*, no. 216105, 2009.

[38] C. Cho, B. Choi, H. Kang, and S. Lee, "Numerical twin image suppression by nonlinear segmentation mask in digital holography.," *Optics express*, vol. 20, no. 20, pp. 22454–64, 2012.

[39] A. Greenbaum, Y. Zhang, A. Feizi, P.-L. Chung, W. Luo, S. R. Kandukuri, and A. Ozcan, "Wide-field computational imaging of pathology slides using lens-free on-chip microscopy," *Science Translational Medicine*, vol. 6, no. 267, pp. 175–267, 2014.

[40] L. Denis, C. Fournier, T. Fournel, and C. Ducottet, "Twin-image noise reduction by phase retrieval in in-line digital holography," in *Wavelets XI, SPIE's Symposium on Optical Science and Technology* (M. Papadakis, A. F. Laine, and M. A. Unser, eds.), p. 59140J, 8 2005.

[41] C. Zuo, J. Sun, J. Zhang, Y. Hu, and Q. Chen, "Lensless phase microscopy and diffraction tomography with multi-angle and multi-wavelength illuminations using a LED matrix," *Opt. Express*, vol. 23, no. 11, pp. 14314–14328, 2015.

[42] W. Luo, A. Greenbaum, Y. Zhang, and A. Ozcan, "Synthetic aperture-based on-chip microscopy," *Light: Science & Applications*, vol. 4, no. 3, p. e261, 2015.

[43] I. Yamaguchi and T. Zhang, "Phase-shifting digital holography," *Optics Letters*, vol. 22, p. 1268, 8 1997.

[44] S. Lai, B. King, and M. A. Neifeld, "Wave front reconstruction by means of phase-shifting digital in-line holography," *Optics Communications*, vol. 173, no. 1-6, pp. 155–160, 2000.

[45] H. Kogelnik, "Coupled Wave Theory for Thick Hologram Gratings," *Bell System Technical Journal*, vol. 48, pp. 2909–2947, 11 1969.

[46] J. H. Hong, "Volume holographic memory systems: techniques and architectures," *Optical Engineering*, vol. 34, p. 2193, 8 1995.

[47] G. Barbastathis, M. Levene, and D. Psaltis, "Shift multiplexing with spherical reference waves.," *Applied optics*, vol. 35, pp. 2403–17, 5 1996.

[48] F.-K. Bruder, F. Deuber, T. Fäcke, R. Hagen, D. Hönel, D. Jurbergs, T. Rölle, and M.-S. Weiser, "Reaction-diffusion model applied to high resolution Bayfol HX photopolymer," p. 76190I, 2 2010.

[49] A. Greenbaum, W. Luo, T.-W. Su, Z. Göröcs, L. Xue, S. O. Isikman, A. F. Coskun, O. Mudanyali, and A. Ozcan, "Imaging without lenses: achievements and remaining challenges of wide-field on-chip microscopy," *Nature Methods*, vol. 9, no. 9, pp. 889–895, 2012.

[50] S. Eisebitt, J. Lüning, W. F. Schlotter, M. Lörgen, O. Hellwig, W. Eberhardt, and J. Stöhr, "Lensless imaging of magnetic nanostructures by X-ray," *Nature*, vol. 432, no. December, pp. 885–888, 2004.

[51] O. Mudanyali, D. Tseng, C. Oh, S. O. Isikman, I. Sencan, W. Bishara, C. Oztoprak, S. Seo, B. Khademhosseini, and A. Ozcan, "Compact, light-weight and cost-effective microscope based on lensless incoherent holography for telemedicine applications," *Lab on a Chip*, vol. 10, no. 11, p. 1417, 2010.

[52] A. C. Sobieranski, F. Inci, H. C. Tekin, E. Comunello, A. V. Wangenheim, and U. Demirci, "Portable Digital in-Line Holography Platform for Sperm Cell Visualization and Quantification," *2014 27th SIBGRAPI Conference on Graphics, Patterns and Images*, pp. 274–281, 2014.

[53] S. Seo, T.-W. Su, A. Erlinger, and A. Ozcan, "Multi-color LUCAS: Lensfree On-chip Cytometry Using Tunable Monochromatic Illumination and Digital Noise Reduction," *Cellular and Molecular Bioengineering*, vol. 1, no. 2-3, pp. 146–156, 2008.

[54] A. Greenbaum, W. Luo, B. Khademhosseinieh, T.-W. Su, A. F. Coskun, and A. Ozcan, "Increased space-bandwidth product in pixel super-resolved lensfree on-chip microscopy," *Scientific Reports*, vol. 3, 4 2013.

[55] W. Bishara, T.-W. Su, A. F. Coskun, and A. Ozcan, "Lensfree on-chip microscopy over a wide field-of-view using pixel super-resolution.," *Optics express*, vol. 18, no. 11, pp. 11181–11191, 2010.

[56] D. Tseng, O. Mudanyali, C. Oztoprak, S. O. Isikman, I. Sencan, O. Yaglidere, and A. Ozcan, "Lensfree microscopy on a cellphone.," *Lab on a chip*, vol. 10, pp. 1787–92, 7 2010.

[57] S. Seo, T.-W. Su, D. K. Tseng, A. Erlinger, and A. Ozcan, "Lensfree holographic imaging for on-chip cytometry and diagnostics," *Lab Chip*, vol. 9, no. 6, pp. 777–787, 2009.

[58] K. Lee and Y. Park, "Quantitative phase imaging unit.," *Optics letters*, vol. 39, no. 12, pp. 3630–3, 2014.

[59] A. Singh, A. Anand, R. Leitgeb, and B. Javidi, "Lateral shearing digital holographic imaging of small biological specimens," *Optics Express*, vol. 20, no. 21, pp. 23617–23622, 2012.

[60] G. Zheng, R. Horstmeyer, and C. Yang, "Wide-field, high-resolution Fourier ptychographic microscopy," *Nature Photonics*, vol. 7, pp. 739–745, 7 2013.

[61] W. Bishara, U. Sikora, O. Mudanyali, T.-W. Su, O. Yaglidere, S. Luckhart, and A. Ozcan, "Holographic pixel super-resolution in portable lensless on-chip microscopy using a fiber-optic array," *Lab on a Chip*, vol. 11, no. 7, p. 1276, 2011.

[62] T.-W. Su, S. O. Isikman, W. Bishara, D. Tseng, A. Erlinger, and A. Ozcan, "Multi-angle lensless digital holography for depth resolved imaging on a chip.," *Optics express*, vol. 18, pp. 9690–711, 4 2010.

[63] S. O. Isikman, W. Bishara, S. Mavandadi, F. W. Yu, S. Feng, R. Lau, and A. Ozcan, "Lens-free optical tomographic microscope with a large imaging volume on a chip," *Proceedings of the National Academy of Sciences*, vol. 108, no. 18, pp. 7296–7301, 2011.

[64] P. Marquet, B. Rappaz, P. J. Magistretti, E. Cuche, Y. Emery, T. Colomb, and C. Depeursinge, "Digital holographic microscopy: a noninvasive contrast imaging technique allowing quantitative visualization of living cells with subwavelength axial accuracy," *Optics letters*, vol. 30, no. 5, pp. 468–470, 2005.

[65] B. Kemper, D. Carl, J. Schnekenburger, I. Bredebusch, M. Schäfer, W. Domschke, and G. von Bally, "Investigation of living pancreas tumor cells by digital holographic microscopy," *Journal of Biomedical Optics*, vol. 11, no. 3, p. 34005, 2006.

[66] A. Anand, V. K. Chhaniwal, N. R. Patel, and B. Javidi, "Automatic identification of malaria-infected RBC with digital holographic microscopy using correlation algorithms," *IEEE Photonics Journal*, vol. 4, no. 5, pp. 1456–1464, 2012.

[67] Z. El-Schich, S. Kamlund, B. Janicke, K. Alm, and A. G. Wingren, "Holography: The Usefulness of Digital Holographic Microscopy for Clinical Diagnostics," in *Holographic Materials and Optical Systems*, InTech, 3 2017.

[68] B. Kemper and G. von Bally, "Digital holographic microscopy for live cell applications and technical inspection," *Applied Optics*, vol. 47, no. 4, pp. A52–A61, 2008.

[69] F. Dubois, C. Schockaert, N. Callens, and C. Yourassowsky, "Focus plane detection criteria in digital holography microscopy by amplitude analysis," *Optics Express*, vol. 14, no. 13, p. 5895, 2006.

[70] B. Rappaz, E. Cano, T. Colomb, J. Kühn, C. Depeursinge, V. Simanis, P. J. Magistretti, and P. Marquet, "Noninvasive characterization of the fission yeast cell cycle by monitoring dry mass with digital holographic microscopy.," *Journal of biomedical optics*, vol. 14, no. 3, p. 034049, 2009.

[71] B. Kemper, A. Vollmer, C. E. Rommel, J. Schnekenburger, and G. von Bally, "Simplified approach for quantitative digital holographic phase contrast imaging of living cells.," *Journal of biomedical optics*, vol. 16, no. February, p. 026014, 2011.

[72] P. Girshovitz and N. T. Shaked, "Compact and portable low-coherence interferometer with off-axis geometry for quantitative phase microscopy and nanoscopy," *Optics Express*, vol. 21, no. 5, p. 5701, 2013.

[73] N. C. Pégard, M. L. Toth, M. Driscoll, and J. W. Fleischer, "Flow-scanning optical tomography," *Lab Chip*, vol. 14, no. 23, pp. 4447–4450, 2014.

[74] F. Dubois and C. Yourassowsky, "Full off-axis red-green-blue digital holographic microscope with LED illumination," *Optics Letters*, vol. 37, no. 12, p. 2190, 2012.

[75] P. Ferraro, G. Coppola, S. D. Nicola, A. Finizio, G. Pierattini, S. De Nicola, A. Finizio, and G. Pierattini, "Digital holographic microscope with automatic focus tracking by detecting sample displacement in real time.," *Optics letters*, vol. 28, no. 14, pp. 1257–1259, 2003.

[76] B. Mandracchia, V. Bianco, Z. Wang, M. Mugnano, A. Bramanti, M. Paturzo, and P. Ferraro, "Holographic microscope slide in a spatio-temporal imaging modality for reliable 3D cell counting," *Lab Chip*, vol. 17, pp. 2831–2838, 2017.

[77] V. Bianco, B. Mandracchia, V. Marchesano, V. Pagliarulo, F. Olivieri, S. Coppola, M. Paturzo, and P. Ferraro, "Endowing a plain fluidic chip with micro-optics: a holographic microscope slide," *Light: Science & Applications*, vol. 6, no. 9, p. e17055, 2017.

[78] M. Frómeta, G. Moreno, J. Ricardo, Y. Arias, M. Muramatsu, L. Gomes, G. Palácios, F. Palácios, H. Velázquez, J. Valin, and L. Ramirez Q, "Optimized setup for integral refractive index direct determination applying digital holographic microscopy by reflection and transmission," *Optics Communications*, vol. 387, no. December 2016, pp. 252–256, 2017.

[79] A. Anand, V. K. Chhaniwal, and B. Javidi, "Imaging embryonic stem cell dynamics using quantitative 3-D digital holographic microscopy," *IEEE Photonics Journal*, vol. 3, no. 3, pp. 546–554, 2011.

[80] P. Langehanenberg, L. Ivanova, I. Bernhardt, S. Ketelhut, A. Vollmer, D. Dirksen, G. Georgiev, G. von Bally, and B. Kemper, "Automated three-dimensional tracking of living cells by digital holographic microscopy.," *Journal of biomedical optics*, vol. 14, no. 1, p. 014018, 2015.

[81] Y.-c. Lin, H.-C. Chen, H.-Y. Tu, C.-Y. Liu, and C.-J. Cheng, "Optically driven full-angle sample rotation for tomographic imaging in digital holographic microscopy," *Optics Letters*, vol. 42, no. 7, p. 1321, 2017.

[82] F. Charrière, A. Marian, F. Montfort, J. Kuehn, T. Colomb, E. Cuche, P. Marquet, and C. Depeursinge, "Cell refractive index tomography by digital holographic microscopy," *Optics Letters*, vol. 31, no. 2, p. 178, 2006.

[83] W. Qu, C. O. Choo, V. R. Singh, Y. Yingjie, and A. Asundi, "Quasi-physical phase compensation in digital holographic microscopy," *Journal of the Optical Society of America A*, vol. 26, p. 2005, 9 2009.

[84] J. K. Wallace, S. Rider, E. Serabyn, J. Kühn, K. Liewer, J. Deming, G. Showalter, C. Lindensmith, and J. Nadeau, "Robust, compact implementation of an off-axis digital holographic microscope," *Optics Express*, vol. 23, no. 13, p. 17367, 2015.

[85] V. Chhaniwal, A. S. G. Singh, R. A. Leitgeb, B. Javidi, and A. Anand, "Quantitative phase-contrast imaging with compact digital holographic microscope employing Lloyd's mirror," *Optics Letters*, vol. 37, no. 24, p. 5127, 2012.

[86] N. Shaked, "Quantitative phase microscopy of biological samples using a portable interferometer," *Optics letters*, vol. 37, no. 11, pp. 2016–2018, 2012.

[87] S. Rawat, S. Komatsu, A. Markman, A. Anand, and B. Javidi, "Compact and field-portable 3D printed shearing digital holographic microscope for automated cell identification," *Applied Optics*, vol. 56, no. 9, p. D127, 2017.

[88] E. C. Shi, J. J. Ng, C. M. Lim, and W. Qu, "Compact lensless digital holographic microscopy using a curved mirror for an enlarged working distance," *Applied Optics*, vol. 55, no. 14, p. 3771, 2016.

[89] D. Claus and J. M. Rodenburg, "Pixel size adjustment in coherent diffractive imaging within the Rayleigh–Sommerfeld regime," *Applied Optics*, vol. 54, p. 1936, 2015.

[90] G. Zheng, S. A. Lee, Y. Antebi, M. B. Elowitz, and C. Yang, "The ePetri dish, an on-chip cell imaging platform based on subpixel perspective sweeping microscopy (SPSM)," *Proceedings of the National Academy of Sciences of the United States of America*, vol. 108, pp. 16889–94, 10 2011.

[91] X. Cui, L. M. Lee, X. Heng, W. Zhong, P. W. Sternberg, D. Psaltis, and C. Yang, "Lensless high-resolution on-chip optofluidic microscopes for Caenorhabditis elegans and cell imaging.," *Proceedings of the National Academy of Sciences of the United States of America*, vol. 105, pp. 10670–5, 8 2008.

[92] M. Lee, O. Yaglidere, and A. Ozcan, "Field-portable reflection and transmission microscopy based on lensless holography," vol. 2, no. 9, pp. 4489–4496, 2011.

[93] A. C. Sobieranski, F. Inci, H. C. Tekin, M. Yuksekkaya, E. Comunello, D. Cobra, A. von Wangenheim, and U. Demirci, "Portable lensless wide-field microscopy imaging platform based on digital inline holography and multi-frame pixel super-resolution," *Light: Science & Applications*, vol. 4, no. 10, p. e346, 2015.

[94] W. Luo, Y. Zhang, A. Feizi, Z. Göröcs, and A. Ozcan, "Pixel super-resolution using wavelength scanning," *Light: Science & Applications*, vol. 5, no. 4, p. e16060, 2015.

[95] Y. Yang, A. Adibi, and D. Psaltis, "Holographic Recording Geometry," *Applied Optics*, 2003.

[96] M. Guizar-sicairos, S. T. Thurman, and J. R. Fienup, "Efficient subpixel image registration algorithms," *Optics Letters*, vol. 33, no. 2, pp. 156–158, 2008.

[97] F. Soulez, E. Thiebaut, A. Schutz, A. Ferrari, F. Courbin, and M. Unser, "Proximity operators for phase retrieval," *Applied optics*, vol. 55, no. 26, pp. 7412–7421, 2016.

[98] L. I. Rudin, S. Osher, and E. Fatemi, "Nonlinear total variation based noise removal algorithms," *Physica D: Nonlinear Phenomena*, vol. 60, pp. 259–268, 11 1992.

[99] R. W. Gerchberg and W. O. Saxton, "A practical algorithm for the determination of phase from image and diffraction plane pictures," *Optik*, vol. 35, no. 2, pp. 237–246, 1972.

[100] J. R. Fienup, "Phase retrieval algorithms: a comparison," *Appl. Optics*, vol. 21, no. 15, pp. 2758–2769, 1982.

[101] T. Latychevskaia and H.-W. Fink, "Resolution enhancement in in-line holography by numerical compensation of vibrations," *Optics Express*, vol. 25, no. 17, p. 20109, 2017.

[102] M. Rostykus, F. Soulez, M. Unser, and C. Moser, "Compact lensless phase imager," *Optics Express*, vol. 25, p. 4438, 2 2017.

[103] M. Elad and H. Y. Or, "A fast super-resolution reconstruction algorithm for pure translational motion and common space invariant blur," *IEEE Transactions on Image Processing*, vol. 10, no. 8, pp. 1187–1193, 2001.

[104] J. W. Goodman, *Introduction to Fourier Optics*. W. H. Freeman, 3 ed., 2005.

[105] M. Rostykus and C. Moser, "Compact lensless off-axis transmission digital holographic microscope," *Optics Express*, vol. 25, p. 16652, 7 2017.

[106] G. Dardikman, N. A. Turko, N. Nativ, S. K. Mirsky, and N. T. Shaked, "Optimal spatial bandwidth capacity in multiplexed off-axis holography for rapid quantitative phase reconstruction and visualization," *Optics Express*, vol. 25, no. 26, p. 33400, 2017.

[107] N. A. Turko, M. Isbach, S. Ketelhut, B. Greve, J. Schnekenburger, N. T. Shaked, and B. Kemper, "Photothermal quantitative phase imaging of living cells with nanoparticles utilizing a cost-efficient setup," *Proceedings of SPIE*, vol. 10074, p. 100740Q, 2017.

[108] C. Fournier, F. Jolivet, L. Denis, N. Verrier, E. Thiebaut, C. Allier, and T. Fournel, "Pixel super-resolution in digital holography by regularized reconstruction," *Applied Optics*, vol. 56, no. 1, pp. 69–77, 2017.

[109] F. Perraut, M. Doménès, H. Grateau, and Q. Josso, "Achieving magnification smaller than 1 in lensless microscopy by illumination with a convergent wavefront," *Opt. Lett.*, vol. 41, no. 22, pp. 5326–5328, 2016.

[110] P. Thevenaz, U. E. Ruttimann, and M. Unser, "A pyramidal approach to subpixel registration based on intensity," *IEEE Transactions on Image Processing*, vol. 7, no. 1, pp. 27–41, 1998.

[111] E. Bostan, E. Froustey, M. Nilchian, D. Sage, and M. Unser, "Variational Phase Imaging Using the Transport-of-Intensity Equation.," *IEEE transactions on image processing : a publication of the IEEE Signal Processing Society*, vol. PP, no. 99, p. 1, 2015.

[112] Z. Jingshan, R. a. Claus, J. Dauwels, L. Tian, and L. Waller, "Transport of Intensity phase imaging by intensity spectrum fitting of exponentially spaced defocus planes," *Optics Express*, vol. 22, no. 9, p. 10661, 2014.

[113] C. Edwards, B. Bhaduri, T. Nguyen, B. G. Griffin, H. Pham, T. Kim, G. Popescu, and L. L. Goddard, "Effects of spatial coherence in diffraction phase microscopy," *Optics Express*, vol. 22, no. 5, p. 5133, 2014.

[114] G. Popescu, "Spatial light interference microscopy (SLIM)," *IEEE Photonic Society 24th Annual Meeting, PHO 2011*, vol. 19, no. 2, p. 797, 2011.

Manon Rostykus

manon.rostykus@epfl.ch

Professional Experience

April 2014– May 2018 **Research Assistant - Laboratory of Applied Photonics Devices, EPFL**, Lausanne, Switzerland

• Analog holography, digital holography, high resolution imaging, compact imager, lensless, multi angle illumination, phase imaging, optical design. Advisor: Prof. Christophe Moser.

Teaching Assistant - Laboratory of Applied Photonics Devices, EPFL, Lausanne, Switzerland

• Master level courses: 'Laser: theory and modern applications' and 'Optics laboratories'.

Board member - EPFL Photonics Chapter (EPC), EPFL, Lausanne, Switzerland

• EPFL organization gathering the photonics community on campus and promoting optical science and technology. Workshops, 'Photonics opportunities and companies in Switzerland', closing ceremony of the International Year of Light, seminars, OSA Centennial ceremony, collaboration with Swissphotonics.

Sept. 2013– Feb. 2014 **Engineering Intern - Carl Zeiss AG Corporate Research and Technology**, Jena, Germany

• Ptychography. Simulations, setting up optical system, characterization, optimization.

Feb. 2013– June 2013 **Research Assistant - Laboratory of Biomedical Optics, EPFL**, Lausanne, Switzerland

• Optical Coherence Microscopy (OCM). Optical design (Zemax), miniaturization.

Sept. 2012– Dec. 2012 **Research Assistant - Laboratory of Biomedical Optics, EPFL**, Lausanne, Switzerland

• Optical Coherence Microscopy (OCM). Mechanics, image processing.

May 2012– Aug. 2012 **Research Intern - Biomedical Photonics Center, Centre National de la Recherche Scientifique (CNRS)**, Orsay, France

• PhotoActivated Localization Microscopy (PALM). Setting up optical system, programing (LabVIEW), image analysis.

2011–2012 **Vice President - Forum de l'Optique, Institut d'Optique**, Palaiseau, France
• French largest career fair in optics and photonics.

2011 **Consultant - Optoservices, Institut d'Optique**, Palaiseau, France
• Confidential engineering consulting for HGH Infrared Systems and ONERA (The French Aerospace Lab).

Educational Background

2014–2018 **PhD** from **Ecole Polytechnique Fédérale de Lausanne (EPFL)**, Lausanne, Switzerland - Photonics

2012–2014 **MSc.** from **Ecole Polytechnique Fédérale de Lausanne (EPFL)**, Lausanne, Switzerland - Photonics and Microengineering

2010–2013 **MSc.** from **Institut d'Optique**, Palaiseau, France - Optics and Photonics

2008–2010 **Classes préparatoires aux Grandes Ecoles** at **Lycée Saint-Louis**, Paris, France - Mathematics, Physics and Engineering Physics

Publications

• Peer-reviewed publication: M. Rostykus, F. Soulez, M. Unser and C. Moser, "Compact lensless phase imager," Optics Express, vol. 25, no. 4, p. 241, 2017.
• Peer-reviewed publication: M. Rostykus and C. Moser, "Compact lensless off-axis transmission digital holographic microscope," Optics Express, vol. 25, no. 14, p. 16652, 2017.
• Peer-reviewed publication: M. Rostykus, F. Soulez, M. Unser and C. Moser, "Compact in-line lensfree digital holographic microscope," Methods, 2017.
• Peer-reviewed publication: M. Rostykus, M. Rossi and C. Moser, "Compact lensless subpixel resolution large field of view microscope," Optics Letters, vol. 43, no. 8, p. 1654, 2018.
• Patent: "Compact side and multi angle illumination lensless imager".
• Patent: "Holographic device or imager".

Presentations

• Poster presentation: "Ultra compact high resolution lensless imager" at Swiss Society for Biomedical Engineering annual meeting, 2015, EPFL, Neuchâtel.
• Presentation: "Flat lensless phase imager" at Photonics West, 2016, Moscone Center, San Francisco.
• Presentation: "Flat lensless phase imager" at Digital Holography & 3-D Imaging, 2016, Heidelberg, Germany.
• Presentation: "High-resolution flat lensless phase imager" at Photonics West, 2017, San Francisco, USA.
• Presentation: "High-resolution flat lensless phase imager" at Photorefractive Photonics, 2017, Qingdao, China.
• Presentation: "High-resolution flat lensless phase imager" at Digital Holography & 3-D Imaging, 2017, Jeju, South Korea.
• Presentation: "Compact lens-free phase microscope" at Face2Phase, 2017, Delft, Netherlands.
• Presentation: "Compact lens-free phase microscope" at Photonics West, 2018, San Francisco, USA.

Posters

• "Ultra-flat lensless microscope imager" at Photonics Day 2014, EPFL, Lausanne, Switzerland.
• "Ultra compact high resolution lensless imager" at Transformations in Optics, workshop 2015, Lorentz Center, Leiden, Netherlands.
• "Ultra-flat lensless microscope imager" at Photonics Day 2015, EPFL, Lausanne, Switzerland.
• "Ultra compact high resolution lensless imager" at Swiss Society for Biomedical Engineering annual meeting, 2015, EPFL, Neuchâtel, Switzerland.
• "Ultra-compact high resolution lensless imager" at Photonics Day 2016, EPFL, Lausanne, Switzerland.
• "Compact lensless off-axis transmission digital holographic microscope" at International School on Computational Microscopy, 2017, Amalfi, Italy.
• "Compact lensless off-axis transmission digital holographic microscope" at Photonics Day 2017, EPFL, Lausanne, Switzerland.

Misc

Languages: French, English, German
Scientific outreach, STEM for children, girls in science
Founding board member of Girls In Tech Switzerland a non-profit association focused on the engagement, education and empowerment of girls and women who are passionate about technology.